TOPICAL REVIEW

Insulators at the ultrathin limit: electronic structure studied by scanning tunnelling microscopy and scanning tunnelling spectroscopy

Silvia Schintke[1] **and Wolf-Dieter Schneider**[2]

[1] National Centre of Competence in Research (NCCR) on Nanoscale Science, Institut für Physik und Astronomie, Universität Basel, Klingelbergstraße 82, CH-4056 Basel, Switzerland
[2] Institut de Physique des Nanostructures, Ecole Polytechnique Fédérale de Lausanne (EPFL), CH-1015 Lausanne, Switzerland

E-mail: Silvia.Schintke@unibas.ch and Wolf-Dieter.Schneider@epfl.ch

Abstract
Considerable progress has been made recently, using scanning tunnelling microscopy (STM), scanning tunnelling spectroscopy (STS) and local density functional theory (DFT), in examining the atomic structure and electronic properties of ultrathin insulating films. This article reviews pertinent results to date with special emphasis on ultrathin MgO films on Ag(001) surfaces. Using STS, the layer-by-layer resolved electronic structure up to 3 ML shows that the band gap of about 6 eV at the MgO surface develops within the first 3 ML confirmed by local density of states (LDOS) calculations. Using model calculations, the atomic species observed in STM on the MgO film are unambiguously identified. These results underline the importance of a combination of local spectroscopy, scanning probe techniques and local density of states calculations for the understanding of matter on the microscopic level.

(Some figures in this article are in colour only in the electronic version)

Contents

1. Introduction: insulators and metal oxides

Insulators, like many metal oxides, are of considerable technological importance, e.g. as support for metal particles in catalysis [1], as insulating barriers in miniaturized electronic circuits, in magnetic tunnel junctions [2] for magnetoelectronics or magnetic data storage, or for the development of a variety of nanodevices based on oxide heterostructures. As the ongoing miniaturization in nanotechnology nowadays already reaches the subnanometre regime in electronic devices [3] a detailed study of the morphology and electronic structure of ultrathin insulating layers is of fundamental interest as well as of technological importance. A wide band gap dielectric spacer layer of accurately controllable thickness, i.e. layer-by-layer, would allow tuning in a controlled manner of the electronic, magnetic and chemical interaction between a metal substrate and atoms, molecules, clusters or boundary layers adsorbed on the dielectric material, opening new perspectives for the local investigation of catalysts, applications in magnetoelectronics, molecular electronics and the development of oxide heterostructure-based nanodevices. Intensive surface science studies have been performed on single crystal metal oxide surfaces [4, 5] and thin films (to circumvent sample charging) [6–10] in order to understand their surface structure and their electronic properties on a microscopic level. For various epitaxial oxide films of *several* monolayer thickness the chemical and electronic properties were found to be representative for their single crystal surfaces [11]. However, the band structure of wide band gap materials might be strongly modified when their size is varied from the molecular regime to macroscopic crystals [12], thus influencing electronic and dielectric properties as well as the chemical reactivities at the surface. Therefore, it is of fundamental interest to explore the changes of the surface electronic structure with respect to layer thickness until the electronic structure of a macroscopic single crystal surface is achieved.

For this attempt the capabilities of scanning tunnelling microscopy (STM) and scanning tunnelling spectroscopy (STS) to determine the geometric and the local electronic structure are ideally suited. However, only very few STS investigations of the electronic structure of thin insulator films have been published so far. The results of the present scanning tunnelling spectroscopy investigations and model calculations are indeed promising for further research as they reveal, e.g. for MgO, that within the first three atomic layers a band gap of about 6 eV establishes, which already corresponds to the value on macroscopic MgO(001) single crystals [13, 14]. In addition ultrathin layers of Al$_2$O$_3$ served recently as a substrate for an STS/STM study of vibrationally resolved fluorescence excited with submolecular precision on supported single molecules [15].

Although no complete and general picture on the thin film electronic structure has yet emerged, several interesting observations in STS and/or STM investigations have recently been made concerning electronic structure and morphology of thin insulator films.

This topical review aims to give an overview of the present studies on the electronic structure of thin films of insulating materials using STM and STS methods. As an introduction a short summary of STM and STS is given in section 2, where different modes of tunnelling spectroscopy are discussed with respect to their application to wide band gap insulators, and examples are presented for the possible origins of chemical contrast in STM images. In the main part of this topical review, we summarize results from literature on systems of ultrathin films of insulating materials, for which information on the electronic structure has been obtained successfully by STM and/or local tunnelling spectroscopy measurements. The system MgO/Ag(001) is the system for which STM and STS has been used in a very detailed way in order to investigate the thin film electronic structure layer by layer [13, 14]. Ultrathin MgO films shall here serve as a model system, and will be discussed in most detail in the last part (section 4) of this topical review.

2. Scanning tunnelling microscopy (STM) and scanning tunnelling spectroscopy (STS)

This section gives a brief summary on scanning tunnelling microscopy (STM) in section 2.1 and scanning tunnelling spectroscopy (STS) in section 2.2, for details see e.g. [16–18] and [17, 19]. These techniques have been used in the past, mainly in order to study the surfaces of metals, semi-conductors and transition metal oxides [20] at an atomic scale. However, even for insulating materials these methods provide a powerful tool to investigate electronic structure and morphology especially, but not exclusively, if the insulators are ultrathin films.

2.1. Scanning tunnelling microscopy (STM)

Scanning tunnelling microscopy, developed in 1981 at IBM Zurich Research Laboratory by Gerd Binnig and Heinrich Rohrer, is based on quantum mechanic tunnelling of electrons through the barrier between the surface of a conducting sample and a sharp metal tip at some 10 Å distance above the surface [21]. Conceptually, the STM of Binnig and Rohrer had its predecessor in the Topografiner of Young *et al* [22]. Applying a bias voltage between tip and sample results in a net tunnel current. When scanning the tip over a surface at constant tunnel current, the displacement of the tip given by the voltages applied to piezo-drives yields a topographic image (constant current image) of the surface. Binnig and Rohrer were the first to resolve monatomic steps and surface reconstructions [23] and also demonstrated later that real space images with atomic resolution can be obtained on metal [24, 25] and semiconductor [26] surfaces.

The invention of STM, for which the Nobel prize in 1986 was awarded to Binnig and Rohrer, marks a breakthrough for the investigation of surfaces and adsorbates on an atomic level. With the STM it has become possible to study locally on the atomic scale e.g. chemisorption [27], epitaxy [28], self-assembled nanostructures, solid–liquid interfaces, biological molecules [29], liquid crystals [30], magnetic structures [31], or superconductor vortices [32].

Apart from imaging, the STM tip also provides a manipulation tool for controlled transfer of single atoms [33], molecules [34, 35] or clusters [36] on a surface. By assembling adsorbates it has become possible to form and characterize single chemical bonds [37], to build artificial nanostructures and to construct nanolaboratories on a surface for the study of quantum interference phenomena [38, 39]. The sum of these facilities is promising for versatile applications concerning fields like miniaturization of electronic circuits and devices, molecular electronics, quantum computers, nanochemistry, or life sciences studies.

A detailed theoretical description of STM is, however, extremely difficult due to the lack of translational symmetry of the tunnel junction. The development of the ideas in

theoretical modelling of STM and STS (section 2.2) is e.g. presented in a recent review article by Drakova [40]. In a generalized form of the one-dimensional model of Tersoff and Hamann [41, 42] for vacuum tunnelling between tip and sample, the tunnel current at a given sample bias $+U$ or $-U$ (for bias voltages near the Fermi energy, i.e. with eU small compared to the work functions Φ_t, Φ_s of tip and sample), and at a given tip–sample separation z, is proportional to the convolution integral of the LDOS of the sample ρ_s and of the tip ρ_t. (The tip–sample separation z is defined as the distance between the surface and the centre of curvature of the effective (locally spherical) tip. In the model of Tersoff and Hamann the tip is described by an unperturbed wavefunction of s-wave character.) Taking into account an energy and bias dependent transmission coefficient T of the tunnel barrier, this leads to the following expression for the current [17, 43]:

$$I \propto \int_0^{eU} \rho_s(E)\rho_t(\pm eU \mp E)T(E, eU)\,\mathrm{d}E$$

with transmission coefficient

$$T(E, eU) = \exp\left(-\frac{2z\sqrt{2m}}{\hbar}\sqrt{\frac{\Phi_s + \Phi_t}{2} + \frac{eU}{2} - E}\right).$$

Thus, electrons with energies in the interval from the Fermi level E_F (corresponding to 0 V sample bias) to the energy eU at the applied sample bias U contribute to the tunnel current. As the tunnel current depends on the surface LDOS $\rho_s(E)$, resonant tunnelling into (or out of) electronic states characteristic for atoms or molecules of the sample surface can reveal chemical sensitivity, and thereby allow *chemical imaging*; for a comprehensive review see [44]. On GaAs(110), Feenstra *et al* [45], have demonstrated that the Ga atoms show strong tunnelling into unoccupied states, whereas the As atoms show strong tunnelling from occupied states, i.e. Ga or As atoms are highlighted in constant current images at a sample bias of +1.9 and −1.9 V, respectively. On metal surfaces, chemical contrast can be obtained in the case of element-specific surface states dominating the tunnel current close to the Fermi level [46], or in certain cases upon adsorption of foreign atoms to the tip apex [47, 48]. Chemical contrast can also be obtained due to *element specific work functions* [49, 50]. If the sample bias exceeds the work function, i.e. when the STM is operated in the field emission regime (Fowler–Nordheim regime [51]), electron standing waves are formed in the vacuum gap between tip and sample. They manifest in *field resonances* of the current [52, 53] (sections 2.2, 4.3.6) as predicted earlier by Gundlach [54]. These oscillations of the tunnel current with bias voltage depend on the local work function and on the image force potential [17], and permit chemical contrast in STM images to be obtained, as demonstrated by Jung *et al* for metals via tunnelling into image states [49]. On insulating films (CaF$_1$, CaF$_2$ on Si(111)) chemical contrast has recently been obtained by resonant tunnelling into the conduction-band minimum [55]. In each of these cases knowledge of the local electronic structure is essential for the interpretation of the observed—in general bias dependent—STM image contrast. This information is obtained by scanning tunnelling spectroscopy, which is the subject of the following section.

2.2. Scanning tunnelling spectroscopy (STS)

As the tunnel current depends on the local density of states of the surface (section 2.1), the voltage dependence in STM can be used to obtain spectroscopic information on the local electronic structure of a surface. This allows e.g. the determination of surface state onsets [56–58], superconductor band gaps [32], electronic band gaps of semiconductor surfaces [59], band onsets in insulating films [55], electronic structure on single atoms [60], or

electronic gaps between highest occupied and lowest unoccupied molecular orbitals (HOMO–LUMO gap) in single molecules. Thus, the STM provides a *local* spectroscopic tool for investigating the electronic structure which in conventional methods of surface science analysis such as e.g. ultraviolet photoelectron spectroscopy (UPS) and inverse photoelectron spectroscopy (IPES) is always integrated over large surface areas. (A recent collection of review articles on applications of scanning tunnelling spectroscopy can be found in [19]. For recent developments in local light emission spectroscopy and photoemission with the STM see [15, 61, 62].) Furthermore, the knowledge of the local electronic structure contains the key information for the interpretation of STM image contrasts (section 2.1).

From a theoretical point of view, Tersoff and Hamann [41, 42] were the first to demonstrate that if the tip wavefunction is described as a single spherical s-type wavefunction, the tunnelling conductivity is simply proportional to the sample LDOS at the Fermi level [40]. Thus, under the assumption that the LDOS of the tip ρ_t is indeed a rather smooth function and for a monotonous transmission coefficient $T(eU)$, differentiation of the convolution integral for the tunnel current (section 2.1) shows that the differential conductance $\frac{dI}{dU}$ is directly related to the LDOS of the sample ρ_s:

$$\frac{dI(eU)}{dU} \propto \rho_s(eU)T(eU).$$

Experimentally, local tunnelling spectra are obtained by adjusting the tip over the surface at some tip–sample separation z as a function of start parameters, $z_0(I_0, U_0)$, and then sweeping the bias voltage U and recording the tunnel current $I(U)$. Modulating the bias voltage during the sweep allows the direct measurement, with a lock-in amplifier, of the differential conductance signal $\frac{dI}{dU}$ apart from the I–U characteristic. The spectroscopic measurement is either performed at constant tip–sample separation, $z_0(I_0, U_0)$, i.e. with open feed-back loop, or—especially for taking spectra over large voltage intervals [63]—by varying the tip–sample separation, z, during the voltage sweep by a linear ramp ($z(U) = z_0 \pm \frac{dz}{dU}$ with $\frac{dz}{dU} =$ constant such that the tip approaches the surface when sweeping the voltage towards the Fermi level) or by maintaining constant the resistance [64] or the current [53]. Depending on the system to be investigated (and the spectroscopic information to be measured) the different modes have their advantages, as summarized in the following.

- (dI/dU) spectroscopic measurements at *constant tip–sample separation* are realized by interrupting the feedback loop during the voltage sweep [59] (or by ramping faster than the cut-off frequency of the feedback loop). This permits taking spectra crossing 0 V and was first used for acquiring I–U curves by Feenstra *et al* [59] in order to determine the band gap between occupied and unoccupied surface electronic states on Si(111)- 2×1.

Due to the exponential bias dependence of the transmission coefficient (section 2.1), the current changes over several orders of magnitude when sweeping over large voltage intervals (several volts) at constant tip–sample separation. Thus, the dynamic range for spectroscopy measurements at constant tip–sample separation is determined by the limitations of I–U converters in the current amplifiers. Attention has to be given to possible artifacts, i.e. gap-like features depending on the set-point parameters may appear in the range where the current drops below the detection limit of the instrument. For STS measurements over large voltage intervals it is therefore more practicable to vary the tip–sample separation during the voltage sweep, i.e. to increase the tip–sample separation at high voltages in order to compensate for the exponential voltage dependence of the transmission coefficient. This is essential for a successful investigation of wide band gap insulator layers by STS.

- dI/dU measurements at *tip–sample separation varied by a linear ramp* were first proposed and performed by Feenstra *et al* [59, 65]. This allows the measurement of

spectroscopic features over a wide voltage range (inclusion of the Fermi level remains, in principle, possible). However, a suitable slope for the linear ramp has to be chosen, being the main practical difficulty for this method, as the absolute tip–sample separation is generally unknown.

- dI/dU measurements at *constant gap resistance* [64, 66] require sweeping the bias voltage and the current set-point simultaneously with the feedback loop turned on, yielding a spectrum proportional to the normalized differential conductance $\frac{U}{I}\frac{dI}{dU}$. This mode of tunnelling spectroscopy was introduced by Kaiser and Jaklevic. They correlated their spectra with photoemission results for Au(111) and Pd(111) [66]. Close to the Fermi level the current diverges (ending up in contact between tip and sample), when maintaining the gap resistance. Thus this spectroscopy mode is not practicable close to the Fermi level.

- dI/dU measurements at *constant current* are realized by operating the feedback loop during the voltage sweep and recording the dI/dU signal with a lock-in amplifier at modulation frequencies above the cut-off frequency of the feedback loop [52, 53]. Again, spectra at voltages close to the Fermi level cannot be obtained. STS at constant current has been performed e.g. for the measurement of resonances appearing at bias voltages beyond the work function of the sample [49, 52, 53] (section 2.1).

Such field resonances were first studied in STS by Becker *et al* on Au(110) [52] and Si(111) 7×7 [67] and by Binnig *et al* on clean and oxygen covered Ni(100) [53]. For oxygen covered Ni(100) a shift of the resonance peaks has been observed, consistent with the increase of the work function. On surfaces which exhibit image-potential surface states [68–70], the resonances appearing in the tunnelling spectra are often also named image states [49], consistent with the influence of the image potential on the tunnelling and field emission probability [17, 71].

Apart from local spectroscopy, the STM has the capability of spectroscopic imaging, which allows the investigation of the spatial distribution of the local density of states on a surface, such as e.g. electron standing waves and electron scattering on atomic scale structures, and steps, impurities or quantum corrals (for a recent review see [19]). Spatially resolved spectroscopic information at a particular bias voltage can be obtained by acquiring the dI/dU signal simultaneously with a constant current image.

Moreover, *inelastic tunnelling* processes may influence the voltage dependence of the tunnel current as reported by Jaklevic and Lambe, who first recorded (non-local) inelastic tunnelling spectra from organic molecules [72]. Recently, single-molecule vibrational spectroscopy of adsorbed acetylene molecules on Cu(110) has been demonstrated [73] by measuring the second derivative $\frac{d^2I}{dU^2}$ of the tunnelling current with respect to the bias voltage in local inelastic electron tunnelling spectroscopy.

These examples illustrate that STS is a very powerful method for a local analysis of the electronic structure on a surface. However, one has to be aware of the limits and inherent difficulties of this method. As the tunnel current depends on the overlap of electronic states between tip and sample (section 2.1), STS is only sensitive to those states which have an overlap with the tip states. Thus, most dominant features in STS do not necessarily correspond to states of highest density. In order to avoid misinterpretation of STS data care has to be taken in measurements that the LDOS of the tip, which sensitively depends on tip adsorbates, is a rather smooth function and does not dominate the measured spectra. Therefore, reliable STS data always demands measurements under various tip conditions; the same applies to the interpretation of bias dependent STM image contrasts.

In our study of MgO on Ag(001) [13, 14], STS was used for the first time for a layer-by-layer-resolved measurement of the local electronic structure of thin insulator films (section 4.3).

It has been shown that the determination of the surface band gap, an interface electronic state and field emission resonances on ultrathin MgO films lead to a coherent interpretation of the corresponding STM images of bias dependent contrast (section 4.3.6). By choosing the bias voltage corresponding to the identified electronic states, one images selectively either the oxide surface, the underlying substrate or the interface (section 4.3.7).

Also for several other systems of ultrathin films of insulating materials, information on the electronic structure has been obtained successfully by STM and/or local tunnelling spectroscopy measurements. We summarize the main results for those systems in the following section.

3. Examples of thin insulators (other than MgO)

In this section we present a brief overview of pertinent investigations of the electronic structure of thin insulating films by STM/STS.

3.1. CaF and CaF$_2$

In recent STS investigations of nanostructures of CaF$_1$ and CaF$_2$ on Si(111) the surface conduction band onset of CaF$_1$ has been determined and was used to demonstrate chemical imaging of insulators [55] (section 2.1). In this case, however, only unoccupied states have been investigated and it is only assumed that the full gap is already formed for the first CaF layer on Si(111); atomic resolution is not reported on these films. The linear arrays of CaF$_2$ nanostructures [55, 74] have been shown to serve as an interesting template for the growth of one-dimensional structures of organic molecules using the distinct local chemical reactivities of a self-organized CaF$_1$/CaF$_2$ stripe pattern [75].

3.2. Al$_2$O$_3$

For the growth of well ordered thin alumina surfaces, various surfaces have been used, including especially different Ni–Al alloy surfaces, i.e. Ni$_3$Al(111) [76, 77], NiAl(111) [78] and NiAl(110) [15, 79], and other metal surfaces, e.g. Re(0001) [11] and recently Nb(110)/sapphire (0001) [80].

3.2.1. Al$_2$O$_3$ on NiAl(110).   For Al$_2$O$_3$/NiAl(110) systematic studies on the growth and reactivity of different metals have been done as reported by Bäumer and Freund [79] and in [81], as well as by Nilius *et al* [82]. When exposing the NiAl(110) surface to oxygen a well ordered 0.5 nm thin aluminium oxide film can be grown [8, 79] that exhibits a stoichiometry and structure compatible with γ-Al$_2$O$_3$ (for a schematic structure model see [82]).

From STM images of Al$_2$O$_3$ islands on NiAl(110) taken at various bias voltages, Bertrams *et al* [83] concluded that the apparent heights reflect the bandgap of alumina (7–8 eV) as determined by electron energy loss spectroscopy (EELS) measurements [84]. Bertrams *et al* observe in STM images an apparent height of the Al$_2$O$_3$ islands which is negligible for voltages below 4 V, and measures 3.5 Å at 4 V.

This system, Al$_2$O$_3$ on NiAl(110), has recently also been used as substrate in measurements of 'vibrationally resolved fluorescence excited with submolecular precision' on single molecules by STM [15]. Qiu *et al* [15] combine the light emission measurements with $\frac{\mathrm{d}I}{\mathrm{d}U}$ and $\frac{\mathrm{d}^2 I}{\mathrm{d}U^2}$. For the alumina film they demonstrate that quenching of the molecular fluorescence due to a metal substrate can be sufficiently suppressed by introducing an ultrathin insulator, by which they achieve directly relating optical spectra of individual molecules to the molecular electronic

structure (measured by scanning tunnelling spectroscopy (STS)) and to the conformation of the molecule (imaged by STM). $\frac{dI}{dU}$ curves of the alumina film were measured at constant height and show for the unoccupied states an onset at about 2 V [15].

3.2.2. Al_2O_3 on Re(0001).   In an STM study of oxide supported Ni particles *I–U* curves of a 3.6 ML Al_2O_3 film grown on Re(0001) indicated a band gap of 6 eV [11] versus 7–8.3 eV determined by EELS on Al_2O_3 (0001) single crystal surfaces independent of various reconstructions [85].

3.2.3. Al_2O_3 on $Ni_3Al(111)$.   In an STM study of Al_2O_3 on Ni_3Al (111), Rosenhahn *et al* [86] investigated the apparent step height of the alumina layer as a function of bias voltage. For positive bias voltages (+1.2–3.8 V), they reported an apparent height of 2.5 Å (versus 5 Å geometric height) observed up to +2.1 V, which increases for higher voltages up to 6 Å observed at 3 V. From the island height measurements, the authors estimate the onset of the conduction band at 2.6 eV above the Fermi level.

In a study on the growth of copper and vanadium on well ordered Al_2O_3-films on $Ni_3Al(111)$, Wiltner *et al* [76] report on the observation of two superstructures which appear in STM images at different bias voltages [86, 87]. Wiltner *et al* showed with their STM experiments, that these superstructures with periodicities of 2.6 and 4.5 nm, observed at +3.2 and +2.3 V, respectively, make the layers promising for use as a template for periodic cluster arrays as they govern the nucleation of the deposited metals.

Recently, the exact lateral coincidence of these superstructures has been studied by Maroutian *et al* [77]. In good agreement with the work of Wiltner *et al* the authors observe in low temperature STM experiments the two superstructures with periodicities of 4.5 nm 2 or 2.6 nm to be prominent at voltages from +2.0 to +2.6 V or at voltages above 3.0 V, respectively. Using STS, Maroutian *et al* [77] ascribe this effect to a lateral variation of the LDOS within the apparent unit cell of the oxide film. In the vicinity of the conduction band edge, they found that the density of empty states is locally enhanced over characteristic points of the unit cell. They propose that a coincidence lattice between film and metallic substrate is at the origin of this modulation of the oxide electronic structure. They identified characteristic steep rises in the dI/dU signal with the onsets of the conduction and valence band respectively.

3.3. NiO

For a study of the growth of NiO on Ni(100) upon oxygen exposure, STM has been used in combination with low-energy-electron diffraction (LEED) [88]. Although STM images show that the oxide island formation mainly takes place at step edges, the images of NiO films have been measured for rather low bias voltage and the existence of a gap could not be concluded from the STM measurements. Furthermore, the authors report that their trials to use the STM in its spectroscopic mode [89] failed due to instabilities caused by oxygen induced changes of the tunnelling tip.

The formation of NiO on Ag(001), providing a smaller lattice misfit than NiO on Ni(100) (misfits of 2% and almost 20% respectively), has been studied by STM [90, 91]. For NiO(100) double layer-islands (as for CoO) on Ag(001), the existence of a band gap has been deduced from current versus voltage curves as well as from STM image contrasts [91]. I/U curves on Ag(001) and NiO double layers have been measured and compared for a set point value of +4 V. The I/U characteristic of NiO shows for bias voltages in the range of −4 V up to about 3 V that the tunnelling current is negligible compared to that on Ag; at a corresponding bias voltage ($U = 1$ V) NiO islands are imaged as depressions at $U = 1$ V. For high voltages

(5 V), NiO islands are imaged in the form of protruding islands. It is argued that at these high bias voltages the electronic states of NiO are accessible. The detailed electronic structure, however, was not studied in these works, and a value of the gap of NiO(100) layers has not been determined.

NiO has a bulk band gap of 4.3 eV [92]. The NiO(001) surface has an empty surface state at 0.6 eV [93, 94]. This surface state has not been observed in the present STM of thin NiO(100) layers, while in an elevated temperature STM study on the single crystal NiO(001) surface structure and its defects sites, atomic resolution images have been obtained at $U \geqslant 0.7$ eV by tunnelling into these empty states, as well as for tunnelling into filled states at $U = -1.3$ V [95].

3.4. CoO

CoO layers have been grown epitaxially on Ag(001) and a band gap has been deduced from current versus voltage curves as well as from STM image contrasts [91, 96]. From bias dependent contrast changes of a CoO double layer the band gap has been estimated to be 2–3.5 eV [97] (versus 2.5 eV for bulk CoO [98]). In a recent study [96], Hagendorf *et al* confirm these measurements by scanning tunnelling microscopy and spectroscopy investigation (recorded maps of I/U spectra). CaO(001) double-layer islands are observed as depressions for bias voltages between −1.5 and +2.2 V bias voltage, while above and below these voltages the islands appear as protrusions. Their numerically derived $(dI/dU)/(I/U)$ spectra show peaks at −1.6 and +2.2 V, which coincide with the voltage dependent contrast reversal in STM images of CoO(001). STM images at bias voltages in the gap (−1.5 to −0.4 V and at +1.5 V) show atomic resolution attributed to tunnelling into states at the metal/oxide interface [96]. CoO(111) layers, on the contrary, show no strong voltage dependent STM contrast; from I/U-STS a finite density of CoO states close to the Fermi level is deduced.

3.5. NaCl

Ultrathin well ordered NaCl layers have been grown successfully and subsequently studied by STM on various substrates, including germanium, aluminium, copper and silver surfaces, e.g. on Ge(100) [99], Al(111) and Al(100) [100], on Cu(100) [101], Cu(111) [102], Cu(211) [103], Cu(311) [104] and Cu(532) [105], as well as on Ag(111) [106].

In a study on the initial growth of NaCl overlayers on Ge(100), Glöckler *et al* [99] report STM images for NaCl films up to a thickness of three atomic layers, giving evidence for the earlier proposed carpet-like growth mode of the NaCl layer over monatomic Ge steps, even for small NaCl islands at submonolayer coverage. The authors report that they were only able to perform STM images by imaging occupied sample states using tip voltages of $U = 1.5$–2.7 V. The authors discuss their observation of lateral atomic resolution for the initial double layer. As UPS data indicate that the band structure of the NaCl double layer, at least for **k** parallel to the surface, is similar to that of the bulk, with the valence band maximum at about 4.2 eV [107], Glöckler *et al* [99] concluded that the tunnelling current is most likely predominantly due to emission from Ge states through the NaCl layer. They suggest therefore that the lateral contrast, showing protrusions at either the Na$^+$ or the Cl$^-$ positions, is due to a perturbation and interaction of the Ge wavefunction(s) by the NaCl layer causing a lateral variation of the tunnelling barrier. The reported apparent heights of the NaCl layers on Ge(001) are positive, but smaller than the corresponding geometric heights (3.8 ± 0.3 Å versus 5.6 Å for the first (double) layer and 2.0 ± 0.3 Å for the second (single) versus 2.8 Å NaCl layer).

A carpet-like growth mode of NaCl at submonolayer coverage is also found on the aluminium, copper and silver substrates. Atomic resolution images of the NaCl(001) layers

on all of these substrates also show a periodicity that corresponds to the positions of one type of ion. The NaCl islands appear for all of these substrates, also with positive apparent height in the STM images.

For ultrathin insulating NaCl layers on Al(111) and Al(100) [100], atomic resolution has been obtained at negative sample bias voltages (−0.5 to −3.0 V), imaging the Cl anions as confirmed by spatially resolved *ab initio* calculations of the local density of states. Decreasing NaCl–NaCl step heights were observed with increasing layer thickness and a maximum thickness of three layers for successful imaging was inferred. However, the gap width of the NaCl films has not been investigated. Apart from the energetically favoured (001) orientation of the NaCl layers, Hebenstreit *et al* [108] reported recently on the growth of polar NaCl islands on Al(111).

NaCl on Cu(111) has been studied by Repp *et al* [102, 104]. Similar to the observations on Ge and Al substrates, the islands are imaged with bright contrast in STM images. Atomic resolution images show, even for bias voltages within the band gap of bulk NaCl, the square lattice corresponding to one type of ion of NaCl(001). dI/dU measurements on the NaCl films show a shift of the prior Cu(111) surface state onset towards higher energies upon adsorption of NaCl which is interpreted as an interface state due to NaCl adsorption [102].

In a recent paper, the adsorption properties of NaCl monolayers and bilayers adsorbed on Cu(311) and Cu(100) have been also investigated theoretically by Olsson *et al* [109] using density functional calculations. These investigations include the calculation of adsorption energies and workfunctions for adsorbed NaCl monolayers and bilayers and are compared to the experimental observations of NaCl layers on copper surfaces [101–105]. For the Cu(311) surface a direct covalent interaction between Cl 3p and Cu d states has been identified.

3.6. Ga_2O_3

In a growth study of gallium oxide on CoGa(100), Pan *et al* [110] resolved in STM images different domains of the (2×1) superstructure formed by β-Ga_2O_3 layers; domain boundaries have been observed to appear as protrusions with a height between 0 and 0.2 nm. The authors report that they did not observe any systematic changes of the STM images with respect to the surface structure and heights of steps and islands when varying the tip voltage between 0.5 and 4 V, and therefore concluded by imaging the top surface of the oxide film. The electronic structure of the gallium oxide has not been studied by means of STM or STS.

3.7. CeO_2

CeO_2 (111) layers have been prepared on Pt(111) by post oxidation of a well ordered Pt–Ce alloy and were imaged by STM [111] and on CeO_2 (111) single crystal surfaces [112]. Berner *et al* [111] reported that imaging with atomic resolution requires a bias voltage in the range of −2 and −3 V and tunnelling currents below 100 pA. The valence band onset of bulk CeO_2 has been measured in XPS at around 2.5 eV below the Fermi level [113].

4. Magnesium oxide (MgO)

MgO is an ionic binary oxide with a direct electronic energy gap of 7.8 eV in bulk MgO [114–118]. Crystalline MgO has a rock salt structure with bulk lattice constant $a = 4.20$ Å [5]. For rock salt oxides, the most stable surface is the *non-polar* (charge neutral) (001) surface [5]. At the MgO(001) surface, the band gap is reduced to 6.2 eV, as demonstrated by electron energy

loss spectra of MgO(001) single crystal surfaces [115, 116]. Band structure calculations show that this is due to an unoccupied surface state [119].

To circumvent sample charging when probing insulators with charged particles, many surface science studies are performed on thin epitaxial films. Low-temperature STM and STS studies of the geometric and electronic structure of magnesium oxide thin films have been performed as a function of layer thickness for MgO deposited on Ag(001) [13, 14]. In the following we describe these studies in more detail, and compare it with STM measurements of other groups on MgO/Ag(001), MgO/Mo(001) and on MgO/Fe(001). We start by reporting on information that has been gained on thin MgO films on Mo(001) (section 4.2) and on Fe(001)(section 4.1).

4.1. MgO on Fe(001)

Thin MgO/Fe(001) films were characterized by I–U curves by Klaua *et al* [120]. For unoccupied states, the authors reported that the tunnelling barrier height depends on the MgO layer thickness, starting from 2.5 eV at 2 ML layers to 3.6 eV at 6 ML. Assuming that the Fermi level lies in the midgap, they concluded that the bandgap increases from 5.0 to 7.6 eV as the MgO film thickness varies from 2 to 6 ML. The observed increase of the tunnel current at 2.5 V is in agreement with our results of dI/dU measurements for 1–3 ML MgO on Ag(001) [13, 14]. For the reactive growth of MgO on Fe(001), Oh *et al* [121] have recently studied the chemical structure of the MgO/Fe(001) interface and have found direct evidence for the formation of an FeO layer in coexistence with the MgO film. The system Fe/MgO/Fe is of great interest for the development of magnetic tunnelling junctions. For a recent review on 'epitaxy, magnetic and tunnelling properties of transition metal/MgO(001) heterostructures' see [122] and references therein.

4.2. MgO on Mo(001)

Ultrathin MgO films have been grown on Mo(001) by evaporating Mg in an oxygen background pressure of $\approx 1 \times 10^{-7}$ mbar in the 200–600 K substrate temperature range [123]. HREELS measurements on those films indicate that the properties of the films (6.8 ML) are essentially identical to bulk, single crystal MgO [124].

STM investigations of MgO/Mo(001) show small grains with average size of 2–6 nm upon deposition at room temperature and larger 3D islands upon deposition at 1100 K [6]. In another STM study domain sizes of several tens of nanometres have been observed on a 3 ML MgO film on Mo(001) [11]. For MgO films of less than 8 ML thickness, stable tunnelling is reported for bias voltages of about 3 V [6]. For bias voltages as low as 2.5 V and for films at least as thick as 5 ML, all MgO step-heights were observed to be multiples of ~2 Å in STM images, corresponding to the geometric height difference (2.1 Å) between adjacent (001) planes of MgO. From the observation of generally more stable tunnelling at positive sample bias as well as from the detection of a higher tunnel current at positive bias in I–U measurements, performed at fix tip–sample separation, it is suggested that 'the Fermi level resides closer to the conduction band minimum in these films' [6]. However, the authors reported that they could not extract an energy gap from the I–U measurements [6]. From I–U curves of a rather thick MgO film (30 ML) on Mo(001), acquired within an STM study of oxide supported Pd particles, a band gap of 5.5 eV [125, 126] has been deduced. However, no local spectroscopy studies are reported for *ultrathin* MgO films on Mo(001).

4.3. MgO on Ag(001)

Electronic structure and chemical properties of the MgO/Ag(001) have been studied recently by UPS and XPS measurements on a single MgO(001) monolayer epitaxially grown on the Ag(001) surface at $\approx$470 K substrate temperature [127, 128], showing that hybridization of the O 2p states with the Ag 5sp states increases the density of states above the Fermi level and determines the chemical bonding at the oxide metal interface. A high chemical reactivity towards H_2O chemisorption is observed on the 1 ML MgO film and has been related to the electronic structure of the interface [128].

The generally most favoured interface geometry between a metal oxide of rock salt structure and the (001) surface of an fcc metal, both exhibiting similar lattice constants, is such that the metal atoms occupy hollow sites, i.e. they continue the fcc lattice of the substrate; O atoms occupy top sites. This is in agreement with theoretical investigations of the interface geometry between Ag(001) and MgO(001) [129–131].

Our work on MgO/Ag(001) represents, to our knowledge, the first layer-by-layer investigation of the electronic structure and morphology of an insulator film by STS and STM measurements. It demonstrates that the electronic structure of the corresponding insulator crystal surface, exhibiting a surface band gap of $\sim$6 eV, is already developed within the first three monolayers (ML).

The experimental procedure for thin film growth on Ag(001) is described in section 4.3.1. STM images of ultrathin MgO films, as typically used for STS measurements, are shown in section 4.3.3. STS results on the local electronic structure of ultrathin MgO films are presented in section 4.3.4 and discussed in relation to results of conventional surface science analysis, i.e. UPS and EELS. The experimental results are supported by *ab initio* calculations of the layer-resolved local density of states (LDOS) using density functional theory (DFT), presented in section 4.3.5. Based on the knowledge of the electronic structure, chemical imaging and selective atomic resolution on the MgO/Ag(001) system are presented in sections 4.3.6 and 4.3.7, respectively.

4.3.1. Experimental set-up. The experiments were performed with a home-built low-temperature STM in an ultra-high vacuum (UHV) chamber (base pressure $<2 \times 10^{-10}$ mbar) equipped with standard facilities for sample preparation [132, 133] and surface analysis by Auger electron spectroscopy (AES) and LEED. For comparison, EELS and angle resolved ($\pm 2°$) UPS were performed [134]. The bias voltages for all STM images and STS data with respect to the sample, i.e. negative (positive) bias corresponds to tunnelling from occupied (into unoccupied) electronic states of the sample. All our STM images have been acquired in constant current mode, recording the variation of tip–sample separation, which is presented as a greyscale STM image. The scanning tips were electro-chemically etched W or Ir wires, sharpened by Ar-sputtering in UHV.

4.3.2. Growth and characterization of thin MgO films on Ag(001). The single crystal Ag(001) surfaces were cleaned by standard cycles of sputtering (Ar$^+$, 20 μA cm^{-2}, 1 keV, 300 K, 30 min) and annealing (800 K, 20 min).

Recently, epitaxial growth parameters have been found for MgO thin film growth on Ag(001) [135]. This system exhibits a smaller lattice misfit between MgO and the metal substrate, i.e. of 2.9% (5.4% for Mo(001) [123]). Unlike Mo(001) where MgO films desorb at 1200–1300 K [123, 124], the low melting point of silver requires sputtering in order to remove a MgO film. As on Mo(001), the MgO/Ag(001) films were prepared by evaporating Mg in an oxygen background pressure [135]. From SPA-LEED measurements on MgO films grown at

various temperatures the authors concluded that the best epitaxial film growth is obtained at around 500 K. For $T < 470$ K, satellites appear in the (1×1) diffraction pattern, attributed to a formation of mosaics with (100) planes tilted in the $\langle 110 \rangle$ directions after deposition of 1 ML. Relating the formation of mosaics (with estimated average size of 7 nm) to the nucleation of islands, the island density in the submonolayer regime is estimated to be $\approx 2 \times 10^{12}$ cm^{-2} [136] for MgO film growth at 350 K.

Following these growth parameters reported by Wollschläger *et al* [135], we have grown thin epitaxial MgO films at 500 K Ag(001) substrate temperature by evaporating Mg in an O_2 partial pressure of 1×10^{-6} mbar using deposition rates of 0.1–1 ML min^{-1}. We cross checked by AES, XPS and LEED the stoichiometry and 1×1 surface crystalline structure of MgO(001) films. The ultrathin MgO films (0.3–5 ML) were studied with the STM at 50 K. For the measurement of local differential conductance spectra (dI/dU versus bias U), which are related to the LDOS [42], we used open feedback conditions with lock-in detection (270 Hz sinusoidal modulation of 5 mV amplitude added to the bias). All features of the spectra were carefully checked for reproducibility with different tunnel currents, tip–sample distances, tip conditions and on various topographically comparable surface regions. For acquiring dI/dU spectra over wide voltage intervals, the tip–sample separation, z, was varied continuously during the voltage sweep in different modes, i.e. by a linear ramp ($\frac{dz}{dU} = $ const) [63], or by keeping constant either the tunnel current or the tunnel resistance [64] (section 2.2). We note that using these modes, band onsets naturally appear as peaks [55, 63]. Although the exact positions of the resonance peaks depend on tunnelling parameters and tip conditions, the same overall behaviour has been found for all these STS modes, i.e. also for dI/dU measurements at constant current and at constant resistance.

4.3.3. Morphology. Figure 1(a) shows an STM image displaying the typical surface geometry at submonolayer coverages of MgO.

After deposition of 0.3 ML MgO (figure 1(a)) two-dimensional square islands of 10–15 nm have nucleated homogeneously on the Ag(001) surface. The density of nucleation centres (determined from figure 1) is $\approx 0.4 \times 10^{12}$ cm^{-2}. From SPA-LEED investigations of MgO films grown at 350 K substrate temperature Wollschläger *et al* estimated an island density of $\approx 2 \times 10^{12}$ cm^{-2} and an average island size of 7 nm in the submonolayer regime [136] (section 1). The lower island density and larger island size observed at 500 K (figure 1(a)) is consistent with an increased adsorbate mobility at elevated temperature. Depositing MgO at 300 K substrate temperature, we observed the formation of small grains and a rather irregular film morphology. Tilt angles of the reported mosaics [136] were not obvious in STM images. However, we did not focus on a detailed growth study of MgO. For thickness-dependent strain in epitaxial MgO layers on Ag(001) in the growth direction and for the change of the in-plane lattice constant as a function of film thickness see [137, 138].

The island edges are preferentially oriented along $\langle 100 \rangle$ substrate directions. This edge orientation corresponds to non-polar edges of MgO (figure 1(c)). Some islands which have nucleated near a silver step edge are embedded in the silver layer of the upper terrace, due to Ag self-diffusion at elevated sample temperature [139, 140]. Thus, the two different island contrasts (i, ii) near a terrace step (figure 1(a)) are indicative of the position and [100] orientation of the terrace step prior to nucleation. The embedded islands show no significant difference in size, indicating that the Ag adatom diffusion does not limit the growth of the MgO islands. Note that silver atoms may also still have diffused *after* MgO deposition. Similar to the formation of CoO and NiO islands on Ag(001) [91], we did not observe Ag incorporation in the oxide islands.

Ag, which has diffused around islands that have nucleated on the lower terrace (i), seems to be confined by the MgO islands (figure 1(a)).
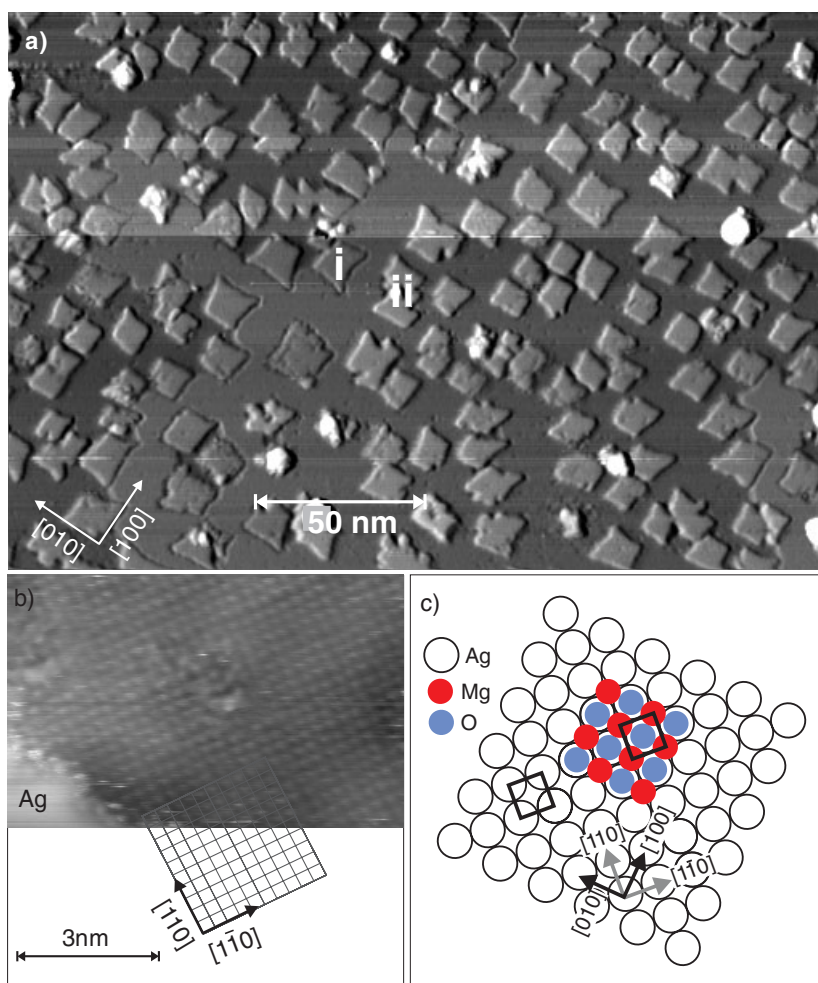
Figure 1. (a) Morphology of MgO thin films at submonolayer coverage: STM image 0.3 ML MgO/Ag(001), $U = 5.0$ V, $I = 1.0$ nA (image lightened from left-hand side for better contrast visibility); (i), (ii) islands nucleated on *lower* and *upper* terrace, respectively—the different island contrasts are indicative of the Ag step position prior to nucleation. (b) Ag(001) atomic resolution *through* an MgO island (cf section 4.3.7) indicating the lattice orientation of the substrate, $U = 30$ mV, $I = 2$ pA (left bottom corner: bare Ag substrate); (c) MgO/Ag(001) growth model, schematic illustration of the most favourable configuration [129–131]: Mg-atoms occupy hollow sites, i.e. they continue the Ag fcc lattice ($a = 4.09$ Å), O-atoms occupy on top sites. The Ag(001) surface unit cell is indicated.

The observed Ag–MgO borders are preferentially oriented along [100] and [010] directions. The Ag has not been seen to mount onto MgO islands. However, practically on all samples we observe some huge islands with an apparent height of sometimes several nanometres and an apparent rather round shape. Their composition and formation is not understood yet, but as these huge islands often tend to cause tip-changes during measurement (as e.g. the one which is seen in the upper part of the image after scan of about 2/3 of the image in figure 1(a)), sample regions free of such islands had to be chosen to perform a series of spectroscopic measurements and imaging with a stable tip. The achieved surface geometry
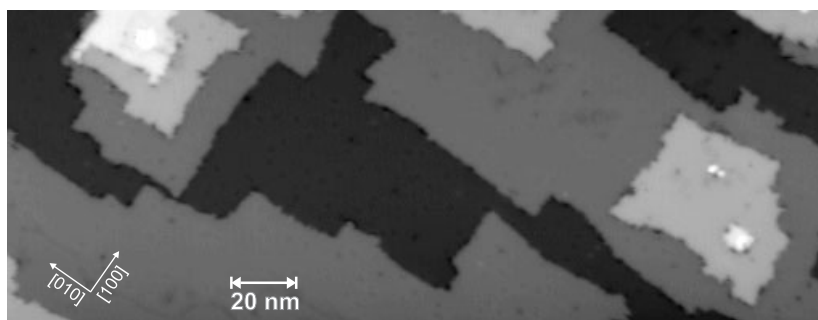
Figure 2. Morphology of MgO thin films: STM image 2 ML MgO/Ag(001), $U = 3.0$ V, $I = 1.0$ nA.

of compact MgO islands coexisting with large uncovered Ag surface regions is ideally suited for comparative dI/dU measurements on MgO and Ag(001) under the same tip conditions.

Figure 1(b) shows atomic resolution of the underlying Ag(001) substrate imaged through the MgO monolayer island (see section 4.3.7). As sample orientation and scan direction were the same for figures 1(a) and (b), the island edge orientation along ⟨100⟩ is directly obvious and corresponds to non-polar edges 1(c). This edge orientation has also been found for MgO on Ag(001) [136] as well as on vicinal Ag(1, 1, 19) [141] in SPA-LEED investigations, whereas Valeri *et al* [142] concluded from their STM measurements a different island edge orientation rotated by 45°, i.e. along ⟨110⟩ directions. These different observations may not be contradictory as recently two types of epitaxial orientations for the growth of alkali halide on fcc metal substrates have been proposed [143].

After deposition of about 2 ML MgO (figure 2) forms terraces of typically 50 nm width and 3D pyramidic islands which allow layer dependent dI/dU measurements. Note that the lowest layer seen in figure 2 corresponds to MgO, as checked by STS (see section 4.3.4). The MgO–MgO steps are preferentially oriented along ⟨100⟩ substrate directions, again corresponding to the non-polar directions of MgO (figure 1(c)).

The ultrathin MgO layers show a low density of defects. From the STM image presented in figure 3 the surface density of defects is estimated to about 0.1% of 1 ML, under the assumption that the defects observed in the (not atomically resolved) image represent isolated point defects (e.g. single oxygen vacancies (F-centres)). Defects play a crucial role in catalytic reactions [144], and are therefore of interest in current research [145]. The STS measurements presented in the following have been performed with the tip positioned above defect free regions of the MgO film surface.

4.3.4. Electronic structure. In this section, experimental results on the local electronic structure of ultrathin MgO films are presented. Figure 4(a) shows representative dI/dU spectra measured with the tip positioned above a 1 ML thick MgO island (free of defects on a scale of 10 nm × 10 nm). At negative sample bias, i.e. for tunnelling out of occupied electronic states, the LDOS increases at −4 V, whereas at positive sample bias (unoccupied states), two structures are detected, around 1.7 and 2.5 V. The energetic positions of these structures depend slightly on the spectroscopic mode (see sections 2.2 and 4.3.2). For dI/dU measurements at constant current they appear at up to 0.3 eV higher energies. Between −4 and +1.7 V, the tunnel current remains finite and the dI/dU spectrum is essentially smooth.

The LDOS increase at −4 V observed with STS on 1 ML MgO compares well with the energetic position of the valence band maximum of MgO(001) observed in normal emission
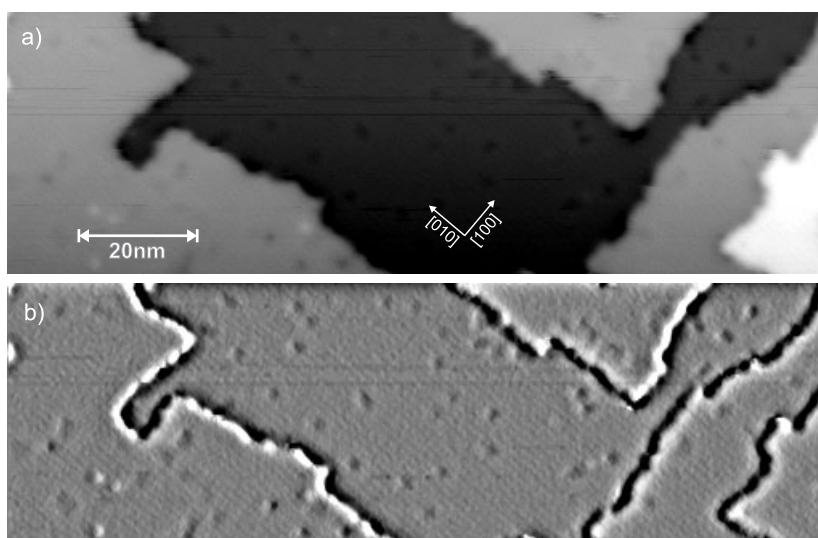
Figure 3. Point defects in a 2 ML MgO/Ag(001) thin film epitaxially grown at 500 K Ag(001) substrate temperature by evaporating Mg in an O_2 partial pressure of 1×10^{-6} mbar using deposition rates of 0.1–1 ML min^{-1} (section 4.3.2): (a) low temperature UHV-STM image at 50 K of 2 ML MgO/Ag(001) (tunnelling parameters $I = 1.0$ nA, $U_{bias} = 3.0$ V applied to the sample), showing MgO terraces. (b) Point defects are visualized for better contrast by highpass filtering of the image (a). The surface density of point defects is $\approx 0.1\%$ of 1 ML.
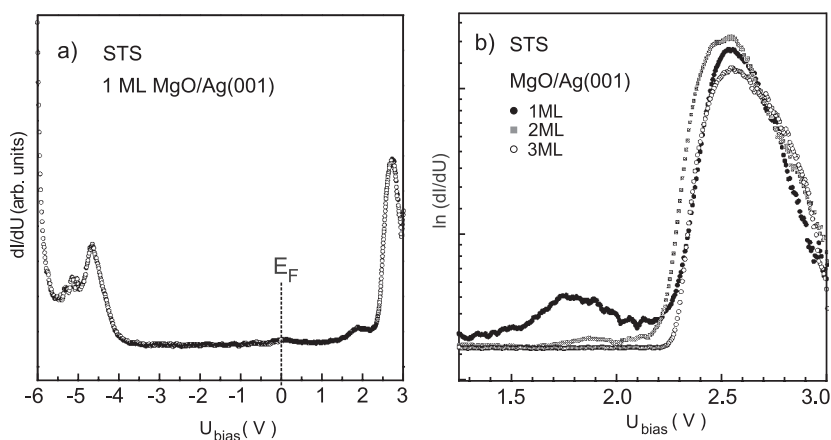
Figure 4. Electronic structure of ultrathin MgO/Ag(001) films as determined by STS—dI/dU spectra (U—sweep interval, tunnelling parameters before opening the feedback loop, linear tip–sample distance variation (approach during sweep to lower bias)): (a) tip placed above a 1 ML MgO island: −6.0 to 0 V, $U_0 = -6.0$ V, $I_0 = 0.2$ nA, $\frac{dz}{dU} = -0.12$ nm V^{-1}; 3.0–0 V, $U_0 = 3.0$ V, $I_0 = 0.2$ nA, $\frac{dz}{dU} = -0.16$ nm V^{-1}; (b) film thickness dependent dI/dU spectra: 3.0–1.0 V, $U_0 = 3.0$ V, $I_0 = 1.0$ nA, $\frac{dz}{dU} = -0.25$ nm V^{-1}.

UPS (figure 5(a), [146]). The intensity of the LDOS peak around 1.7 V observed in STS for 1 ML MgO diminishes for 2 ML and is no longer detectable for an MgO film of 3 ML (figure 4(b)). We note that at the chosen set-point value the MgO layers appear with their geometric height in STM images (see section 4.3.6). Furthermore the three spectra of
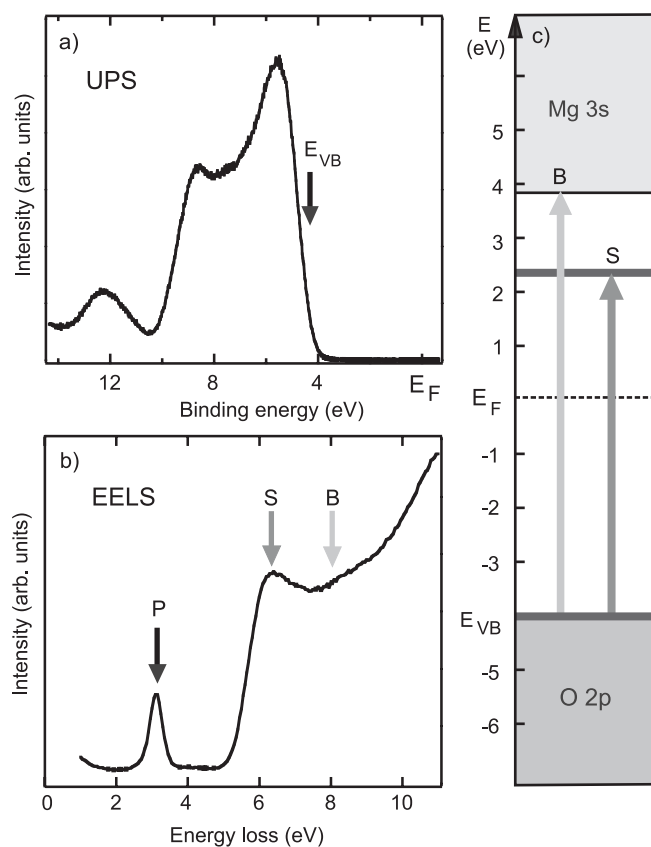
Figure 5. Electronic structure of a 10 ML stoichometric MgO(001)/Ag(001) film as determined by UPS and EELS: (a) He II normal emission spectrum, the valence band onset is indicated. (b) EEL spectrum ($E_p = 30$ eV): Ag–MgO interface plasmon excitation (P) [118, 134], lowest interband transition at the MgO(001) surface (S), bulk interband transition (B). (c) MgO(001) energy level scheme derived from (a) and (b).

figure 4(b) have been acquired with identical dz/dU ramps. Consequently, the relative distance between tip and Ag-substrate for the three spectra differs by the MgO step height. Therefore, we attribute the thickness dependent diminishing feature to the electronic structure of the MgO–Ag interface [128]. According to recent LDOS calculations, this peak corresponds to Ag states which lie in a forbidden energy range for propagation into MgO and are rapidly damped for increasing oxide film thickness [147].

In contrast, the high local density of unoccupied states around 2.5 eV does not decrease with film thickness and, consequently, is identified with MgO states [5, 148]. We deduce for MgO(001) the energy level scheme illustrated in figure 5(c) from the UPS spectrum (figure 5(a)) of a 10 ML MgO film, which fixes the valence band maximum at about 4 eV below the Fermi level, and from the EELS spectrum (figure 5(b)) of the same film, which shows the energy losses corresponding to the interband transitions in MgO bulk and at the MgO(001) surface of 7.8 eV (B) and 6.2 eV (S) [115, 116, 118, 149], respectively.

Thus, we attribute the onset of the 2.5 eV peak observed in STS to the onset of the MgO(001) empty surface state band [115, 119]. Combining the local dI/dU observation of the occupied and unoccupied LDOS on the ultrathin MgO films (figure 4) with the conventional
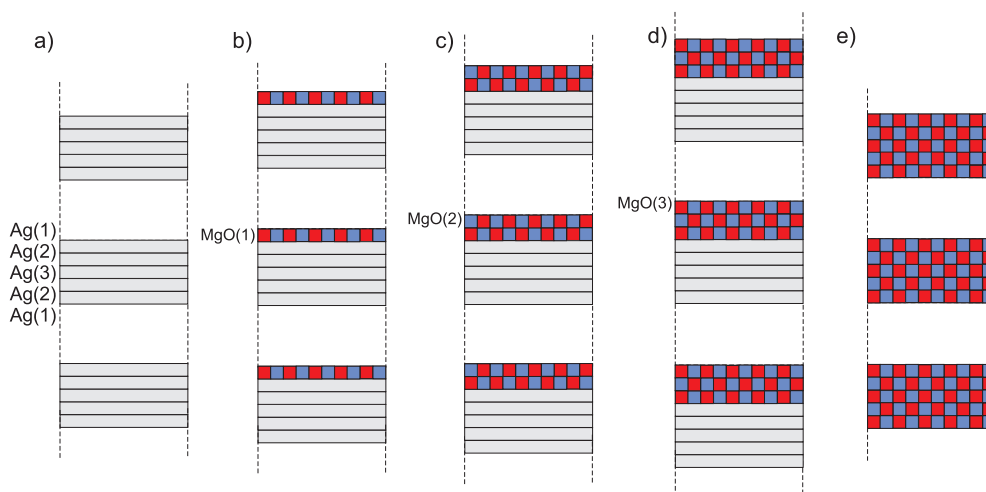
Figure 6. Schematic illustration of slab geometries used for DFT-calculations in periodic boundary conditions (separation by a vacuum layer): (a) 5 ML Ag(001) slab, (b) 1 ML MgO/Ag(001), (c) 2 ML MgO/Ag(001), (d) 3 ML MgO/Ag(001), (e) 5 ML MgO(001) slab.

surface science measurements on thick MgO films (figure 5), we conclude that the electronic structure of an MgO(001) single crystal surface develops within the first three monolayers. Already 1 ML MgO shows the band onsets (gap of 6 eV) reminiscent of the MgO(001) single crystal surface. Apart from an interface electronic structure at +1.7 V, spectra within the gap essentially reflect the exponential bias dependence of the tunnel current (section 2) of the Ag(001) substrate. At 3 ML coverage the electronic structure at the MgO surface shows no contribution from interface states, but corresponds to the electronic structure of an MgO(001) single crystal surface.

4.3.5. Comparison with theory: layer-resolved LDOS of MgO. First principle calculations based on DFT yielded the layer-resolved LDOS as a function of the number n of adsorbed MgO layers ($0 \leqslant n \leqslant 3$) [13]. The results have been obtained using the ABINIT code (http://www.pcpm.ucl.ac.be/abinit). In these calculations, a vacuum layer of 0.9 nm is used to separate each system from its repeated image in the z direction. Tests show that the results do not change using supercells with vacuum layers up to 2 nm. A 288 k-points set is used to sample the surface Brillouin zone (SBZ), which reduces by symmetry to a set of 42 independent k-points in the irreducible SBZ wedge. The total energies of both MgO and Ag bulk systems are well converged using a plane wave cutoff of 70 Ryd (used in all calculations). The pseudopotentials used to model the ionic cores [150] have been generated with the fhi98PP code [151]. Considering full ionic relaxation, test calculations on symmetric systems, where the MgO layers were adsorbed at both sides of the Ag slab, lead substantially to the same results.

The Ag substrate was modelled by a five-layer slab in periodic boundary conditions. The different slab geometries used for DFT calculations are illustrated in figure 6. The O atoms of the first MgO layer are positioned on top of the Ag(001) surface atoms, which is the most favourable configuration [129–131] (see figure 1(c)).

In figure 7, we report the LDOS calculated in the plane of the first atomic layer in each system, and compare the surface layer LDOS of 1–3 adsorbed MgO layers (figures 6(b)–
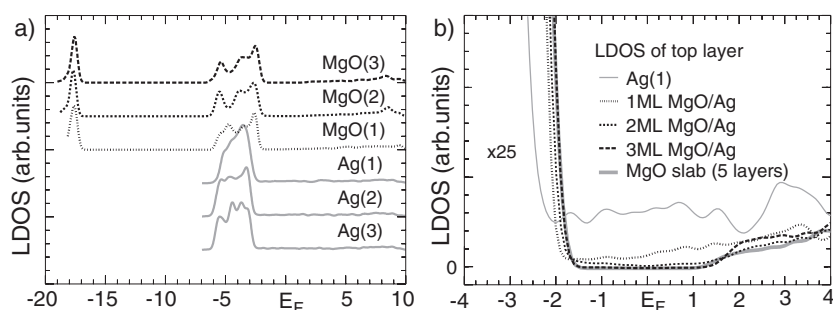
Figure 7. Layer-resolved LDOS calculated with DFT-GGA: (a) Ag(1), Ag(2), Ag(3): LDOS at different layer positions from the surface(1) to the middle(3) in a five-layer Ag-only slab in periodic boundary conditions; MgO(1), MgO(2), MgO(3): LDOS of the surface layer in case of 1, 2, 3 layers MgO, respectively, adsorbed on the five-layer Ag-only slab. (b) Surface layer LDOS in case of 0–3 layers (blow up of (a)) and surface LDOS of a five-layer MgO-only slab (for slab geometries see figure 6).

(d)) and a five-layer pure MgO slab (figure 6(e)). The features of the calculated LDOS for the bare Ag(001) surface (Ag(1), figure 7(a)) and for the surface covered by 1–3 layers MgO/Ag(001) (MgO(n), $n = 1, 2, 3$) correspond qualitatively to those in the UPS spectra (not shown), the occupied states showing the Ag 4d band and the O 2p states. The calculated k-resolved LDOS for the 1 ML MgO system shows that screening of the Ag states by the MgO is considerably more efficient at the surface Brillouin zone boundary than at Γ. Consequently, the states at Γ determine the minimum gap width, in agreement with the electronic structure of MgO [5, 117, 119]. In the gap, the average surface LDOS decays exponentially with the number of adsorbed MgO layers (by about 25% per layer), shown in figure 7(b). This is consistent with the observation of a black island contrast when tunnelling at bias voltages in the gap (figure 12(a), section 4.3.6). Increasing the MgO film thickness up to three layers produces a surface band gap corresponding to that of the five-layer pure MgO slab, which is representative for the MgO(001) surface. The absolute gap value is generally underestimated in LDA [152], also found for MgO [119]. This is also the case for our calculated energy gap for bulk MgO at the equilibrium lattice constant, in agreement with [119]. The surface electronic gap of the five layer pure MgO slab (calculated within the LDA) is also underestimated (figure 7, [152]). The *difference* between the surface and bulk electronic gaps is, however, in good agreement with its experimental value (figure 5(a), [115, 116, 118, 149]). This result matches very well the experimental findings (figures 4(a), (b)).

Recently, Kiguchi *et al* [138] performed EELS and UPS measurements on ultrathin MgO films grown on Ag(001). Their EELS results shows that the band gap energy does not change for MgO thickness from 1 to 20 ML, indicating that the band gap energy of a 1 ML thick MgO film adjacent to a metal substrate is the same as that of a MgO(001) surface. This finding is in excellent agreement with our STS results [13, 14]. Furthermore, Kiguchi *et al* [138] were able to explain the observed upward shift of the valence band edge with decreasing film thickness by the image charge screening of a hole created by photoionization in the presence of the metal substrate.

4.3.6. Chemical contrast in STM images. The knowledge about the electronic structure of MgO islands, obtained from STS measurements and theory, allows a better understanding of the observed image contrast and interpretation of the STM images of the MgO films, as discussed in this and the following section (sections 4.3.6, 4.3.7).
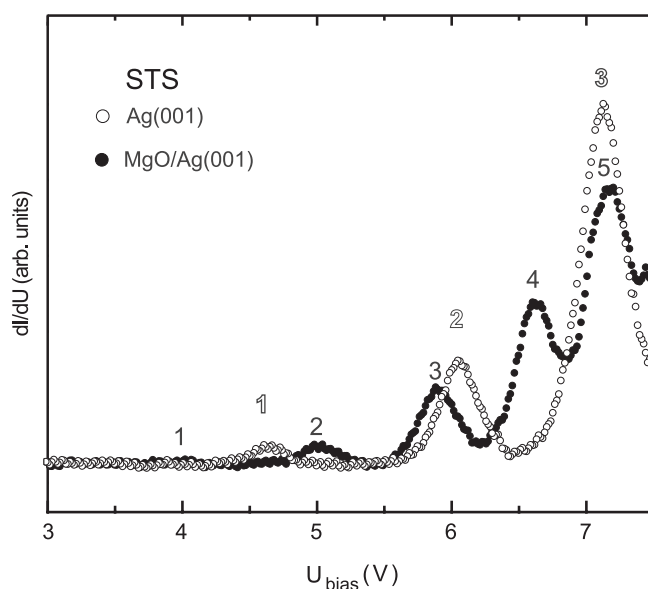
Figure 8. Ag(001) field resonance states: (○) tip above Ag(001), (●) tip above 1 ML MgO island; 7.5–3.0 V, $U_0 = 7.5$ V, $I_0 = 0.2$ nA, $\frac{dz}{dU} = -0.20$ nm V^{-1} (approach during sweep to lower bias).

For metals it has been shown that chemical contrast in STM images can be provided by image states [49] (section 2.2). In order to explore whether this also applies to metal–insulator systems, we performed STS measurements on samples of submonolayer coverages of MgO at bias voltages higher than those already presented before (section 4.3.4). Figure 8 shows differential conductance spectra measured at bias voltages above 3 V, which exhibit oscillations due to the first field resonance states. Their energetic position depends on whether the tip is positioned above an MgO island or the silver surface (between islands). The different energetic positions of the resonances found on MgO and Ag allow chemical imaging, i.e. an enhanced contrast leading to a clear distinction between the oxide and the metal when scanning at appropriate positive sample bias. This is especially interesting to easily identify MgO embedded in the surface layer of Ag(001) (section 4.3.3). For STM images at a sample bias of, e.g. 5 V (figure 1), which corresponds to the energetic position of the second field resonance state when tunnelling through 1 ML MgO (figure 8), the 1 ML MgO islands adsorbed on top of Ag(001) appear clearly higher (0.30 ± 0.01 nm versus 0.21 nm geometric height) than the Ag–Ag steps (0.20 nm), as shown in figure 9(a) presenting scan profiles of the STM image of figure 1.

When the tip is placed above an MgO island the resonance peaks observed in the spectra (figure 8) shift towards lower energies. In general, the energetic position of field emission resonances depends on the local work function and on the image force potential [17] (section 2.2). The direction of the observed shift on MgO is consistent with the *reduced work function* which we observe in UPS (of about 0.4 eV) for a 1 ML MgO/Ag(001) film. In terms of image states, a shift towards lower energies is expected for a reduced field between tip and metal substrate. The Ag(001) surface exhibits image states [70, 153] with zero field positions 3.90, 4.26, 4.35 eV known from two photon photoemission spectroscopy (2PPES) [153]. Analogous to the argument for Ni(001) [53], the electric field between tip and sample causes, due to the Stark effect, a shift and an expansion of the image state spectrum to higher energies
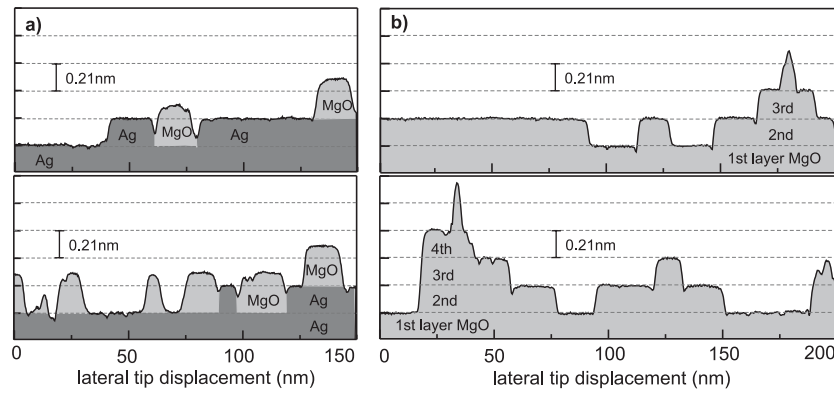
Figure 9. Scan profiles of STM images: (a) submonolayer coverage (figure 1, $U = 5.0$ V, $I = 1.0$ nA): apparent MgO island height 3.0 ± 0.1 Å; (b) 2 ML MgO coverage (figure 2, $U = 3.0$ V, $I = 1.0$ nA) apparent MgO–MgO step heights correspond to their geometric height of 2.1 Å.
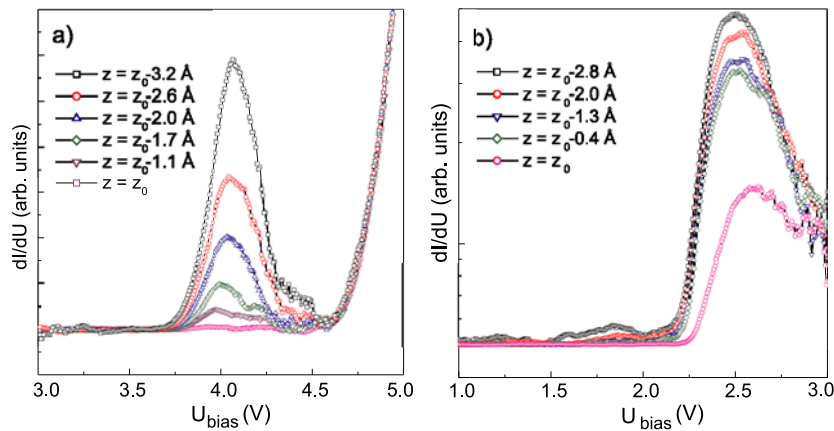
Figure 10. Field dependence of spectral features on a 1 ML MgO island: dI/dU spectra at varied tip–sample separation, varied by a linear ramp; the relative tip–sample distance is indicated with respect to the bias of the observed peak. (a) The field resonance state for decreasing tip–sample separations ($U_0 = 5.0$ V, $I_0 = 1.0$ nA, $\frac{dz}{dU} =$ constant) shifts to higher energies, due to the increased electric field; (b) the surface conduction band stays rather unaffected by variations of the tip–sample separation ($U_0 = 3.0$ V, $I_0 = 1.0$ nA, $\frac{dz}{dU} =$ constant).

in the dI/dU spectra of Ag(001) (figure 8). Thus, in the case of a MgO adlayer, where the resonances are observed at lower energies in dI/dU spectra, the electric field may be reduced by the MgO adlayer.

We discuss two possible ways in which the field may change. Firstly, the electric field is changed due to the variation of the tip–Ag(001) separation when adjusting the tip on either MgO or Ag, at given set-point parameters for taking dI/dU spectra. This difference in tip–Ag(001) separation is given by the apparent height of a 1 ML MgO island in an image at the chosen set-point parameters, and becomes maximal in images taken at a bias corresponding to a field resonance on MgO (3.0 Å at 5 V, figure 9(a)). Using 5 V as set-point, dI/dU spectra are measured above an MgO island for different tip–sample separations (figure 10(a), dI/dU measured in open feed back-loop condition, tip–sample distance varied by a linear ramp). Consistent with an increased field at reduced tip–sample separation, the first resonance peak

shifts to higher energies (figure 10(a)), but does not shift to the position found on uncovered Ag(001), even when reducing the tip–sample separation by more than ≈ 3 Å (corresponding to the apparent island height at set-point parameters). Figure 10(b) shows the field dependence of the surface conduction band onset. As expected, its position stays rather unaffected by decreasing the tip–sample separation. Thus, the geometric effect of an increased tip–Ag(001) separation is of minor contribution to the field resonance shift observed between MgO and Ag (figure 8).

Secondly, the MgO layer may act as a dielectric reducing the electrical field between tip and silver substrate. To evaluate this, further STS studies would be useful, investigating field resonance positions as a function of layer thickness. This might allow better separation and estimation of the contribution to the field emission resonances of both effects, the modified work function and that of the image state potential, which may be screened by MgO acting as dielectric.

Thus, a detailed picture of the contributions of different effects causing the field resonance shift observed on MgO cannot be given yet. However, it has been demonstrated that scanning at a bias voltage corresponding to a resonance position on MgO considerably enhances the STM image contrast of MgO islands, and that therefore chemical contrast in STM images of a metal–insulator system can be obtained via field resonances.

Chemical contrast of the insulator islands is also obtained due to the electronic gap structure of the MgO film, determined in STS (section 4.3.4) and LDOS calculations (section 4.3.5) leading to a consistent interpretation of the observed image contrasts.

Within the gap (-4 to $+2.5$ V), no states of the MgO are available for tunnelling, but the MgO reduces exponentially (see above, figure 7(b)) the probability of tunnelling into the substrate, and the islands appear as depressions (figures 11(b)–(e), 12(a)).

Thus, for bias voltages in the gap the underlying substrate is imaged *through* the MgO adlayer (section 4.3.7).

For bias voltages outside the gap, the islands appear with bright contrast (figures 11 (a), (f)), as tunnelling in or out of states of the MgO film is possible.

At higher coverage the apparent MgO–MgO step heights are found to correspond to their geometric height when tunnelling into MgO states. Figure 9(b) shows e.g. scan profiles obtained at 3.0 V sample bias measured on a sample of 2 ML MgO coverage (figure 2), demonstrating for up to four layers an MgO interlayer spacing of 0.21 nm. This agrees with observations made earlier on MgO/Mo(001) films at $\geqslant 5$ ML coverage and bias voltages $\geqslant 2.5$ V [6]. With the appearance of equidistant layers, the MgO seems clearly different to the case of NaCl on Al(111) [100], where diminishing step heights are observed for increasing layer thickness. However, on NaCl STM measurements were performed at rather low bias voltages (-0.5 to -3 V) while the gap of the ultrathin NaCl films is not known.

Additional STM measurements at bias voltages in the gap on multilayer films of MgO would be interesting for comparison. Due to the lack of MgO electronic states within the gap and the exponential reduction of the Ag LDOS with MgO adlayer thickness, shown in theory (section 4.3.5), it is expected that the contrast also inverts for multilayers, i.e. highest geometric layers should appear deepest in STM images, while the underlying substrate is imaged through the MgO. An equidistant apparent interlayer spacing near the Fermi level would experimentally verify the exponential reduction of the Ag LDOS by MgO adlayers. On a 1 ML MgO film imaging of the underlying substrate *through* the MgO is even possible with atomic resolution as will be shown in the next section.

4.3.7. Atomic resolution on and through the insulator film. The results of the STS investigations of the electronic structure of ultrathin MgO films allow not only a consistent
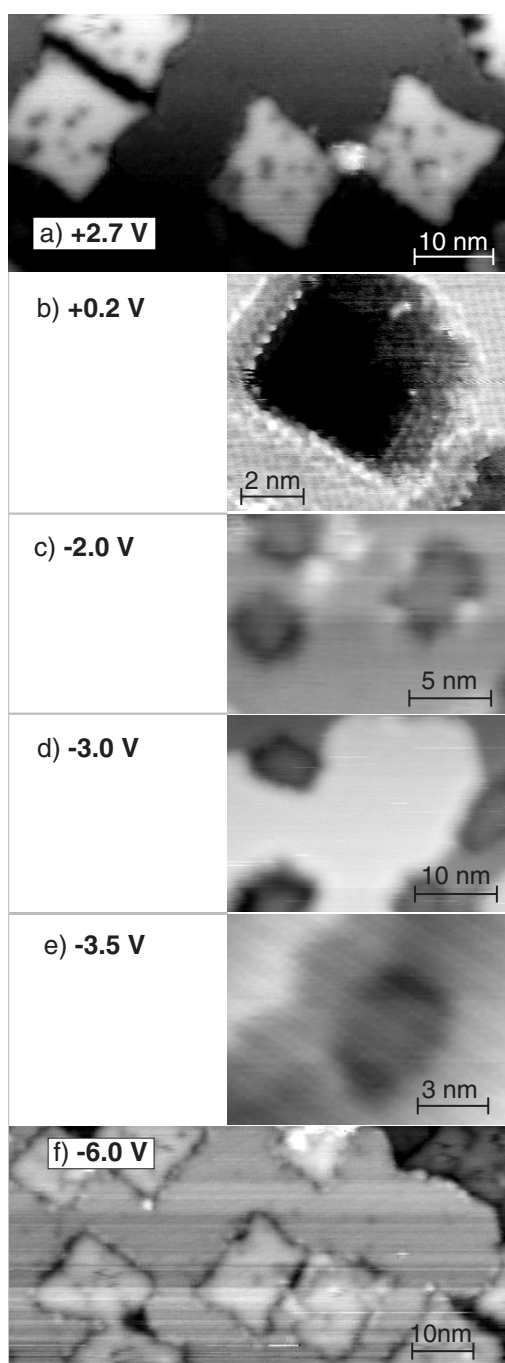
Figure 11. MgO islands imaged at bias voltages beyond the gap appear as protrusions (bright contrast (a) and (f)), at bias voltages within the gap MgO islands appear as depressions (dark contrast (b)–(e)): (a) tunnelling into unoccupied states of MgO ($U = 2.7$ V, $I = 0.3$ nA); (b) atomic resolution on Ag(001) aside the MgO island ($U = 0.2$ V, $I = 5.0$ nA); (c) $U = -2.0$ V, $I = 0.5$ nA; (d) $U = -3.0$ V, $I = 0.5$ nA; (e) $U = -3.5$ V, $I = -3.5$ nA; (f) tunnelling out of occupied states ($U = -6.0$ V, $I = 0.2$ nA) of MgO (embedded islands).

a)

Ag

Ag

b)

[1̄10]

[110]

3 nm

c)

Ag
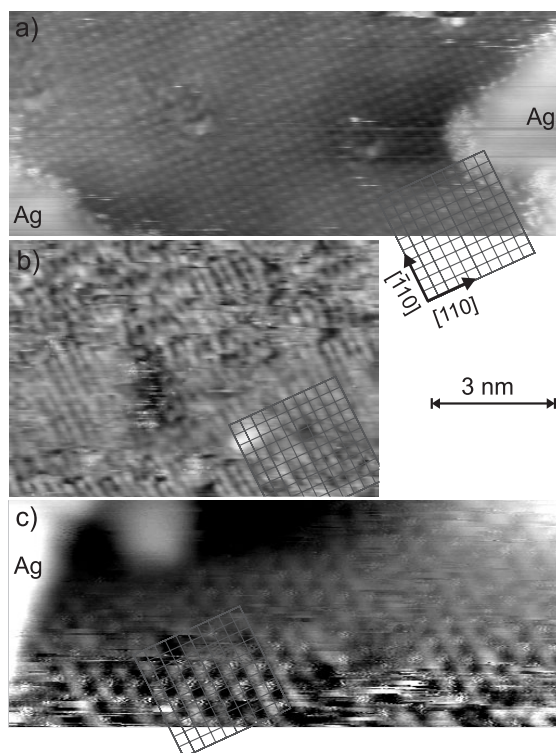
Figure 12. High resolution STM images: (a) Ag(001) atomic resolution *through* a 1 ML MgO island, $U = 30$ mV, $I = 2$ pA (left bottom corner: bare Ag substrate); (b) atomic resolution of the 1 ML MgO layer (one type of the ions is resolved), $U = 2.5$ V, $I = 50$ pA; (c) high resolution image at the interface state showing a c(2×4) superstructure of the charge distribution, $U = 1.7$ V, $I = 2$ pA.

interpretation of the image contrast, which can be used for chemical imaging, but also provide the possibility selectively imaging the MgO surface or the underlying silver substrate by choosing an appropriate bias voltage.

Figure 12(a) shows an STM image taken on a 1 ML MgO island at a bias voltage close to the Fermi level. At this sample bias, in the gap of MgO, the MgO reduces the probability of tunnelling, i.e. the island appears with dark contrast (figure 12(a); section 4.3.6), while a remaining density of Ag states (section 4.3.5) contributes to the tunnel current into the substrate. Therefore, the image (figure 12(a)) shows atomic resolution of the square Ag substrate lattice, imaged *through* the MgO layer (section 4.3.3). The atomic resolution is achieved at a current of only 2 pA, which is not sufficiently high to get simultaneously atomic resolution on the bare metal surface aside the island. The defects which are seen in the lattice may either be defects of the substrate or (point-) defects in the film (figure 3) causing interference with the tunnel current from the substrate. STS studies on MgO point defects as well as subsequent imaging at bias voltages within and beyond the gap might give further insight.

At $+2.5$ V, tunnelling into states of the MgO layer (MgO surface state band, see section 4.3.4) becomes possible. Thus, the STM image figure 12(b) taken on a 1 ML MgO island, atomically resolves the MgO layer. The lattice contains local defects and appears not to be perfectly arranged, which may be due to strain in the film, or most probably to the influence of the interface state on the image formation at the applied bias voltage. The image suggests

a slight double row formation of MgO, which should be investigated in detail in further STM measurements. The observed surface lattice constant (SLC) has twice the value of the SLC of MgO, thus only one type of ion is imaged. This corresponds to STM observations on atomically resolved NaCl films [99, 100]. Hebenstreit *et al* [100] identified the imaged ion by means of spatially resolved calculations of the LDOS of NaCl layers on aluminium.

Recently, Stengel and co-workers [147] calculated the integrated LDOS from the Fermi level up to 3 eV in order to simulate our STM experiment. The data are taken from a symmetrical LDA calculation with an 11 layers Ag slab and 1 ML MgO adsorbed on both sides of the slab. The positions of the MgO, O and two interfacial Ag layers have been fully relaxed.

Figures 13(a), (b) show two cutplanes of the integrated LDOS. The first cutplane (figure 13(a)) is a MgO(100) one, passing through the surface oxygen (black filled circles) and the magnesium (white filled circle), as well as through the substrate silver atoms (grey circles). The second cutplane is a (001) one, parallel to the surface. The vertical position of this cutplane is indicated in the (100) picture as a dashed line. The positions of the underlying Mg and O surface atoms are also indicated (white and black filled circles, respectively).

Figures 13(a), (b) clearly show that the maxima of the integrated density of unoccupied states are located above the Mg ions and the minima above the oxygen ions. Therefore, the protrusions observed in the experimental STM image (figure 12(b)) have to be identified with the locations of the Mg-atoms. Note that in figure 12(a) the silver region of the integrated density of unoccupied states is completely white (maximum) as a consequence of a substantial contribution from the silver 5sp band. Interestingly there is a rather strong maximum in the region corresponding to oxygen $2p_z$ orbitals. This means that a non-negligible density of states corresponding to O $2p_z$ is pushed above the Fermi level upon interaction with Ag. This is in good agreement with photoemission results from Altieri *et al* [128].

In this context a recent DFT calculation by Sgroi *et al* [154] is interesting. These authors adopted a periodic slab model, consisting of six layers of Ag covered on both sides with a MgO monolayer. It was found that the presence of the Ag substrate has an appreciable influence on the structural and electronic properties of the oxide, but only at the interface. In the most stable configuration of the O ions directly above the Ag atoms, the Mg atoms in the hollow sites, the surface is corrugated, and there is a net transfer of electrons from the overlayer to the metal leading to a substantial reduction of the work function of the metal, which corresponds to our experimental results *et al* [13, 14]. Furthermore, these authors found the maxima of the charge density above the Mg atoms and the minima above the O atoms.

Tunnelling at a sample bias of +1.7 V, where an electronic structure related to the interface has been observed in the STS measurements (section 4.3.4), yields images exhibiting a pattern of c(2 × 4) superstructure, as shown in figure 12(c). Within the islands, domains rotated by 90° of this c(2 × 4) pattern are observed (not shown). From STM studies of adlayers the observation of Moiré patterns is reported, caused by the lattice misfit and a laterally modulated relative geometric position of the atoms of substrate and adsorbate [100, 155]. However, the observed c(2 × 4) pattern of the MgO/Ag(001) system is only found for the bias voltage that from the STS results has been associated to an interface electronic state. This state below the MgO surface conduction band onset might be a metal-induced gap state [156] due to coupling of quantum states in the insulator band and the conduction band of the metal [157]. Further STM/STS investigations may clarify if an analogue state and pattern can be found close to the MgO valence band edge. Measuring dI/dU maps (especially at +1.7 V sample bias) and spatially resolved calculation of the LDOS might give insight into the formation of the apparent superstructure. Voltage dependent imaging with atomic resolution of substrate, interface and MgO layer at identical sample regions may clarify the origin of this superstructure analogous to recent experiments on ultrathin Al_2O_3 films [77].
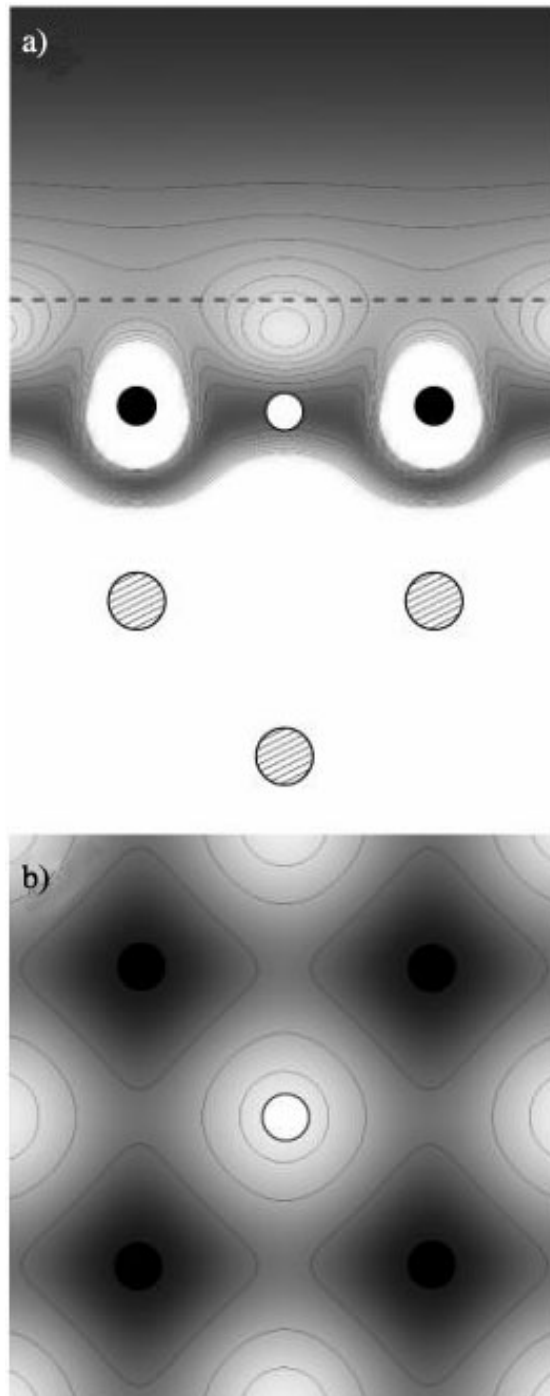
Figure 13. Integrated LDOS from E_F to 3.0 V (unoccupied states) for 1 ML MgO on Ag(001). Atom positions: Mg, white filled circles, O, black circles, Ag, grey circles; greyscale: white, maximum, black, minimum of the LDOS; (a) xz-cutplane of Mg(100), (b) xy-cutplane above MgO(001) at the z-position indicated by the dashed line of figure (a) [147].

5. Conclusion and outlook

The investigation of the morphology and local electronic structure of ultrathin MgO films leads to the following new results. Ultrathin epitaxial films with a low surface density of defects have been grown successfully, leading to 2D islands of 10–15 nm size for submonolayer coverages and to 3D growth with formation of terraces of up to, typically, 50 nm at coverages of 2–3 ML (section 4.3.3).

Layer-resolved differential conductance (dI/dU) measurements reveal that at a film thickness of three ML a gap of about 6 eV is already formed corresponding to that of the MgO(001) single crystal surface (section 4.3.4). This finding is confirmed by layer-resolved calculations of the local density of states (LDOS) based on density functional theory (DFT) (section 4.3.5). STS measurements of the first MgO layer show the electronic band onsets at −4 and +2.5 V, corresponding to the values found for the MgO(001) surface on macroscopic single crystals and thick films. This observation has been made on large MgO terraces of 1 ML height as well as on 1 ML MgO islands of 10–15 nm; dI/dU spectra on smaller islands may give information on any influence of the island size. In addition, an electronic state at +1.7 V observed in dI/dU spectra up to 2 ML thickness, has been related to the interface electronic structure. According to recent calculations [147], the following picture emerges. The bottom of the MgO surface conduction band has the character of an image state [116]. It penetrates little into the material and is localized in the vacuum region [147] where it is detected at 2.5 eV in the STS measurements [13, 14] (section 4.3.4). As the observed energetic position of this state is independent of the MgO layer thickness, the surface electronic band gap remains constant down to the monolayer limit, an experimental confirmation of the ideas of Cox and Williams [116].

Knowledge of the electronic gap structure, as well as the observation of field resonances on MgO and Ag in STS measurements, allows a consistent interpretation of observed STM image contrasts and yields chemical imaging on the insulator-metal surface. We note that for diamond, a bulk insulator, Bobrov *et al* [158] recently demonstrated that resonant tunnelling into field emission states can even be used for atomic scale STM imaging of the surface of bulk insulators.

For bias voltages within the gap, the dark appearance of the islands is attributed to an exponential reduction of the Ag LDOS by the MgO adlayers, found in DFT calculations. For an experimental verification of this exponential behaviour, STM measurements on apparent step heights of multilayer MgO films at bias voltages within the gap are suggested. For tunnelling at bias voltages beyond the gap, i.e. where electronic states of the MgO are available, submonolayer islands are observed with bright contrast, and multilayer islands show MgO–MgO step heights of 2.1 Å corresponding to the geometric MgO interlayer spacing.

In addition atomic resolution has been obtained selectively on the MgO film and the underlying substrate (imaged *through* an MgO island) by choosing the bias voltage corresponding to the MgO surface state band onset (+2.5 V) and close to the Fermi level, respectively (section 4.3.7). Atomic resolution on the MgO images one type of ion, corresponding to the Mg cations for imaging unoccupied states, as shown by calculations of the integrated LDOS above the surface [147] (section 4.3.7).

At the bias voltage of +1.7 V, which corresponds to an interface electronic state [147] observed in STS (section 4.3.4), a c(2 × 4) pattern is observed in STM images. Further investigations are necessary in order to understand the image pattern formation, and to deduce if it has a geometric origin, e.g. related to misfit compensation of the oxide film.

Further interesting investigation of the MgO films could address the observed (point-) defects, e.g. dI/dU measurement of the electronic structure or a controlled creation of defects

by the STM tip. This may help to explore their nature which is of considerable interest in current research due to the fundamental role that defects play for chemical reactions on surfaces or metal oxide supported clusters.

In summary, the results of the investigations yield a consistent picture between the local electronic structure of ultrathin MgO films and the information that is obtained in STM images. The STS investigations and model calculations reveal that within the first three atomic layers of MgO, a band gap of about 6 eV develops corresponding to the value found for MgO(001) single crystals. By simply choosing accurately the number of dielectric spacer layers (1–3 ML) of these wide band gap materials, the electronic, magnetic and chemical interaction between a metal substrate and atoms, molecules, clusters or boundary layers adsorbed on the dielectric material may be tuned in a controlled manner. This opens new perspectives for the local investigation of catalysts, for applications in magnetoelectronics [159], and for the development of oxide heterostructure-based nanodevices [3].

Acknowledgments

References

[1] Ertl G, Knözinger H and Weitkamp J (ed) 1997 *Handbook of Heterogeneous Catalysis* vol 1–5 (Weinheim: Wiley) ISBN 3-527-29218-8

[2] Moodera J S, Nassar J and Mathon G 1999 Spin-tunneling in ferromagnetic junctions *Annu. Rev. Mater. Sci.* **29** 381–432

[3] Chau R, Kavalieros J, Roberds B, Schenker R, Lionberger D, Barlage D, Doyle B, Arghavani R, Murthy A and Dewey G 2000 30 nm physical gate length CMOS transistors with 1.0 ps n-MOS and 1.7 ps p-MOS gate delays *IEDM Proc. IEEE Int. Electron Devices Mtg (Dec. 2000)* (Piscataway, NJ: IEEE) (http://www.intel.com/research/silicon/ieee/ieee6.htm)

[4] Henrich V E 1985 The surfaces of metal oxides *Rep. Prog. Phys.* **48** 1481–541

[5] Henrich V E and Cox P A 1994 *The Surface Science of Metal Oxides* (Cambridge: Cambridge University Press)

[6] Gallagher M C, Fyfield M S, Cowin J P and Joyce S A 1995 Imaging insulating oxides: scanning tunneling microscopy of ultrathin MgO films on Mo(001) *Surf. Sci.* **339** L909–13

[7] Freund H J, Kuhlenbeck H and Staemmler V 1996 Oxide surfaces *Rep. Prog. Phys.* **59** 283–347

[8] Bäumer M, Libuda J and Freund H-J 1997 in *Chemisorption and Reactivity on Supported Clusters* ed R M Lambert and G Pacchioni (Dordrecht: Kluwer–Academic)

[9] Xu C and Goodman D W 1997 in *Handbook of Heterogeneous Catalysis* vol 1–5, ed G Ertl, H Knözinger and J Weitkamp (Weinheim: Wiley) ISBN 3-527-29218-8

[10] Campbell C T 1997 Ultrathin metal films and particles on oxide surfaces: structural, electronic and chemisorptive properties *Surf. Sci. Rep.* **27** 1–111

[11] Street S C, Xu C and Goodman D W 1997 The physical and chemical properties of ultrathin oxide films *Annu. Rev. Phys. Chem.* **48** 43–68

[12] Alivisatos A P 1996 Semiconductor clusters, nanocrystals, and quantum dots *Science* **217** 933–7

[13] Schintke S, Messerli S, Libioulle L, Pivetta M, Patthey F, Stengel M, De Vita A and Schneider W-D 2001 Insulator at the ultrathin limit: MgO on Ag(001) *Phys. Rev. Lett.* **87** 276801

[14] Schintke S 2002 Oxygen and ultrathin metal–oxide films on silver: morphology and electronic structure *PhD Thesis* Université de Lausanne 2001 (Berlin: Dr Köster) ISBN 3-89574-452-2
    Schintke S 2001 *Wissenschaftliche Schriftenreihe Physik* Band 71 ISSN 1431-0228

[15] Qiu X H, Nazin G V and Ho W 2003 *Science* **299** 542

[16] Amelinckx S, van Dyck D, van Landuyt J and van Tendeloo G (ed) 1997 *Handbook of Microscopy: Methods II* (Weinheim: VCH) ISBN 3-527-292280-2

[17] Wiesendanger R 1994 *Scanning Probe Microscopy and Spectroscopy: Methods and Applications* (Cambridge: Cambridge University Press) ISBN 0-521-41810-0

[18] Wiesendanger R (ed) 1998 *Scanning Probe Microscopy—Analytical Methods* (*NanoScience and Technology*) (Berlin: Springer) ISBN 3-540-63815-6

[19] Schneider W-D (ed) 2000 Scanning tunneling spectroscopy *J. Electron Spectrosc. Relat. Phenom.* **109** 1–224 (special issue)

[20] Bonnel D A 1998 Scanning tunneling microscopy and spectroscopy of oxide surfaces *Prog. Surf. Sci.* **57** 187–252

[21] Binnig G and Rohrer H 1982 Scanning tunneling microscopy *Helv. Phys. Acta* **55** 726–35

[22] Young R, Ward J and Scire F 1971 Observation of metal–vacuum–metal tunneling, field emission, and the transition region *Phys. Rev. Lett.* **27** 922–4

[23] Binnig G, Rohrer H, Gerber Ch and Weibel E 1982 Surface studies by scanning tunneling microscopy *Phys. Rev. Lett.* **49** 57–61

[24] Binnig G, Rohrer H, Gerber Ch and Weibel E 1983 (111) Facets as the origin of reconstructed Au(110) surfaces *Surf. Sci.* **131** L379–84

[25] Baró A M, Binnig G, Rohrer H, Stoll H, Baratoff A and Salvan F 1984 Real-space observation of the 2 × 1 structure of chemisorbed oxygen on Ni(110) by scanning tunneling microscopy *Phys. Rev. Lett.* **52** 1304–7

[26] Binnig G, Rohrer H, Gerber Ch and Weibel E 1983 7 × 7 reconstruction on Si(111) resolved in real space *Phys. Rev. Lett.* **50** 120–3

[27] Wolkow R and Avouris Ph 1988 Atom-resolved surface chemistry using scanning tunneling microscopy *Phys. Rev. Lett.* **60** 1049–52

[28] Chambliss D D, Chiang S and Wilson R J 1991 Scanning tunneling microscopy studies of metal/metal epitaxial growth *Mater. Res. Soc. Symp. Proc.* **229** 15–25

[29] Amrein M, Stasiak A, Gross H, Stoll E and Travaglini G 1988 Scanning tunneling microscopy of recA-DNA complexes coated with a conducting film *Science* **240** 514

[30] Foster J S and Frommer J E 1988 Imaging of liquid crystals using a tunneling microscope *Nature* **333** 542–5

[31] Wiesendanger R, Güntherodt H J, Güntherodt G, Gambino R J and Ruf R 1990 Observation of vacuum tunneling of spin-polarized electrons with the scanning tunneling microscope *Phys. Rev. Lett.* **65** 247–50

[32] Hess H F, Robinson R B, Dynes R C, Valles J M Jr and Waszczak J V 1989 Scanning-tunneling-microscope observation of the Abrikosov flux lattice and the density of states near and inside a fluxoid *Phys. Rev. Lett.* **62** 214–6

[33] Eigler D M and Schweizer E K 1990 Positioning single atoms with a scanning tunneling microscope *Nature* **344** 524–6

[34] Becker R S, Golovchenko J A and Swartzentruber B S 1987 Atomic-scale surface modifications using a tunneling microscope *Nature* **325** 419

[35] Foster J S, Frommer J E and Arnett P C 1988 Molecular manipulation using a tunneling microscope *Nature* **331** 324–6

[36] Messerli S, Schintke S, Morgenstern K, Sanchez A, Heiz U and Schneider W-D 2000 Imaging size-selected silicon clusters with a low temperature scanning tunneling microscope *Surf. Sci.* **465** 331–8

[37] Lee H J and Ho W 1999 Single bond-formation and characterization with a scanning tunneling microscope *Science* **286** 1719–22

[38] Manoharan H C, Lutz C P and Eigler D M 2000 Quantum mirages formed by coherent projection of electronic structure *Nature* **403** 512–5

[39] http://www.almaden.ibm.com/vis/stm/gallery.html

[40] Drakova D 2001 Theoretical modelling of scanning tunneling microscopy, scanning tunneling spectroscopy and atomic force microscopy *Rep. Prog. Phys.* **64** 205–90

[41] Tersoff J and Hamann D R 1983 Theory and application for the scanning tunneling microscope *Phys. Rev. Lett.* **50** 1998–2001

[42] Tersoff J and Hamann D R 1985 Theory of the scanning tunneling microscope *Phys. Rev.* B **31** 805–13

[43] Tromp R M 1989 Spectroscopy with the scanning tunneling microscope: a critical review *J. Phys.: Condens. Matter* **1** 10211–28

[44] Jung T A, Himpsel F J, Schlittler R R and Gimzewski J K 1998 Chemical information from scanning probe microscopy and spectroscopy *Scanning Probe Microscopy—Analytic Methods* (*NanoScience and Technology*) ed R Wiesendanger (Berlin: Springer) ISBN 3-540-63815-6

[45] Feenstra R M, Stroscio J A, Tersoff J and Fein A P 1987 Atom-selective imaging of the GaAs(110) surface *Phys. Rev. Lett.* **58** 1192–5

[46] Mo Y W and Himpsel F J 1994 Spectroscopic signature of Cu on W(110) from scanning tunneling microscopy and inverse photoemission *Phys. Rev.* B **50** 7868–71

[47] Schmid M, Stadler H and Varga P 1993 Direct observation of surface chemical order by scanning tunneling microscopy *Phys. Rev. Lett.* **70** 1441–4

[48] Johnson K E, Chambliss D D, Wilson R J and Chiang S 1993 Growth and morphology of partial and multilayer Fe thin films on Cu(100) and the effect of adsorbed gases studied by scanning tunneling microscopy *J. Vac. Sci. Technol.* A **11** 1654–60

[49] Jung T, Mo Y W and Himpsel F J 1995 Identification of metals in scanning tunneling microscopy via image states *Phys. Rev. Lett.* **74** 1641–4

[50] Wiesendanger R, Bode M, Pascal R, Allers W and Schwarz U D 1996 Issues of atomic-resolution structure and chemical analysis by scanning probe microscopy and spectroscopy *J. Vac. Sci. Technol.* A **14** 1161

[51] Fowler R H and Nordheim L 1928 Electron emission in intense electric fields *Proc. R. Soc.* **119** 173–81

[52] Becker R S, Golovchenko J A and Swartzentruber B S 1985 Electron interferometry at crystal surfaces *Phys. Rev. Lett.* **55** 987–90

[53] Binnig G, Frank K H, Fuchs H, Garcia N, Reihl B, Rohrer H, Salvan F and Williams A R 1985 Tunneling spectroscopy and inverse photoemission: image and field states *Phys. Rev. Lett.* **55** 991–4

[54] Gundlach K H 1966 Zur berechnung des tunnelstroms durch eine trapezförmige potentialstufe *Solid-State Electron.* **9** 949–57

[55] Viernow J, Petrovykh D Y, Kirakosian A, Lin J-L, Men F K, Henzler M and Himpsel F J 1999 Chemical imaging of insulators by STM *Phys. Rev.* B **59** 10356–61

[56] Crommie M F, Lutz C P and Eigler D M 1993 Imaging standing waves in a two-dimensional electron gas *Nature* **363** 524–7

[57] Hasegawa Y and Avouris Ph 1993 Direct observation of standing wave formation at surface steps using scanning tunneling spectroscopy *Phys. Rev. Lett.* **71** 1071–4

[58] Li J, Schneider W-D and Berndt R 1997 Local density of states from spectroscopic scanning tunneling microscope images: Ag(111) *Phys. Rev.* B **56** 7656–9

[59] Feenstra R M, Thompson W A and Fein A P 1986 Real-space observation of π-bonded chains and surface disorder on Si(111) 2×1 *Phys. Rev. Lett.* **56** 608–11

[60] Crommie M F, Lutz C P and Eigler D M 1993 Spectroscopy of a single adsorbed atom *Phys. Rev.* B **48** 2851–4

[61] Ushioda S 2000 Scanning tunneling microscope (STM) light emission spectroscopy of surface nanostructures *J. Electron Spectrosc. Relat. Phenom.* **109** 169–82

[62] Gray S M 2000 Photoemission with the STM *J. Electron Spectrosc. Relat. Phenom.* **109** 183–96

[63] Feenstra R M and Mårtensson P 1988 Fermi-level pinning at the Sb/GaAs(110) surface studied by scanning tunneling spectroscopy *Phys. Rev. Lett.* **61** 447–50

[64] Kaiser W J and Jaklevic R C 1987 Scanning tunneling microscopy study of metals: spectroscopy and topography *Surf. Sci.* **181** 55–68

[65] Stroscio J A, Feenstra R M and Fein A P 1986 Electronic structure of the Si(111) 2×1 surface by scanning-tunneling microscopy *Phys. Rev. Lett.* **57** 2579–82

[66] Kaiser W J and Jaklevic R C 1986 Spectroscopy of electronic states of metals with a scanning tunneling microscope *IBM J. Res. Dev.* **30** 411

[67] Becker R S, Golovchenko J A, Hamann D R and Swartzentruber B S 1985 Real-space observation of surface states on Si(111) 7×7 with the tunneling microscope *Phys. Rev. Lett.* **55** 2032–4

[68] Johnson P D and Smith N V 1983 Image-potential states and energy-loss satellites in inverse photoemission spectra *Phys. Rev.* B **27** 2527–30

[69] Straub D and Himpsel F J 1984 Identification of image-potential surface states on metals *Phys. Rev. Lett.* **52** 1922–4

[70] Reihl B, Frank K H and Schlittler R R 1984 Image-potential and intrinsic surface states on Ag(100) *Phys. Rev.* B **30** 7328–31

[71] Sommerfeld A and Bethe H 1933 *Handbuch der Physik* vol 42/2, ed H Flügge (Berlin: Springer) p 450

[72] Jaklevic R C and Lambe J 1966 Molecular vibration spectra by electron tunneling *Phys. Rev. Lett.* **17** 1139–40

[73] Stipe B C, Rezaei M A and Ho W 1998 Single-molecule vibrational spectroscopy and microscopy *Science* **280** 1732–5

[74] Viernow J, Petrovykh D Y, Men F K, Kirakosian A, Lin J-L and Himpsel F J 1999 Linear arrays of CaF_2 nanostructures on Si *Appl. Phys. Lett.* **74** 2125–7

[75] Rauscher H, Jung T A, Lin J-L, Kirakosian A, Himpsel F J, Rohr U and Müllen K 1999 One-dimensional confinement of organic molecules via selective adsorption on CaF_1 versus CaF_2 *Chem. Phys. Lett.* **303** 363–7

[76] Wiltner A, Rosenhahn A, Schneider J, Becker C, Pervan P, Milun M, Kralj M and Wandelt K 2001 Growth of copper and vanadium on a thin Al_2O_3-film on Ni_3Al *Thin Solid Films* **400** 71–5

[77] Maroutian T, Degen S, Becker C, Wandelt K and Berndt R 2003 Superstructures and coincidences of a thin oxide film on a metallic substrate: A STM study *Phys. Rev.* B **68** 155414

[78] Franchy R, Masuch J and Gassmann P 1996 *Appl. Surf. Sci.* **93** 31

[79] Bäumer M and Freund H-J 1999 *Prog. Surf. Sci.* **61** 127

[80] Dietrich Ch, Boyen H-G and Koslowski B 2003 Characterization of ultrathin insulating Al_2O_3 films grown on Nb(110)/sapphire(0001) by tunneling spectroscopy and microscopy *J. Appl. Phys.* **94** at press

[81] Lambert R M and Pacchioni G (ed) 1997 *Chemisorption and Reactivity on Supported Clusters* (Dordrecht: Kluwer–Academic)

[82] Nilius N, Cörper A, Bozdech G, Ernst N and Freund H-J 2001 Experiments on individual alumina-supported adatoms and clusters *Prog. Surf. Sci.* **67** 99–121

[83] Bertrams Th, Brodde A and Neddermeyer H 1994 *J. Vac. Sci. Technol.* B **12** 2122

[84] Jaeger R M, Libuda J, Bäumer M, Homann K, Kuhlenbeck H and Freund H-J 1998 *J. Electron Spectrosc. Relat. Phenom.* **64/65** 217

[85] Gautier M, Duraud J P, Van L P and Guittet M J 1991 Modifications of α-Al_2O_3(0001) surfaces induced by thermal treatments or ion bombardment *Surf. Sci.* **250** 71–80

[86] Rosenhahn A, Schneider J, Kandler J, Becker C and Wandelt K 1999 *Surf. Sci.* **433–435** 705

[87] Rosenhahn A, Schneider J, Becker C and Wandelt K 2000 *J. Vac. Sci. Technol.* A **18** 1923

[88] Bäumer M, Kappus D, Kuhlenbeck H, Freund H-J, Wilhelmi G, Brodde A and Neddermeyer H 1991 *Surf. Sci.* **253** 116–28

[89] Berghaus Th, Brodde A, Neddermeyer H and Tosch St 1988 *Surf. Sci.* **193** 235

[90] Bertrams Th and Neddermeyer H 1996 Growth of NiO(100) layers on Ag(100): characterization by scanning tunnelling microscopy *J. Vac. Sci. Technol.* B **14** 1141–4

[91] Sebastian I, Bertrams T, Meinel K and Neddermeyer H 1999 Scanning tunnelling microscopy on the growth and structure of NiO(100) and CoO(100) thin films *Faraday Disc.* **144** 129–40

[92] Sawatzky G A and Allen J W 1984 *Phys. Rev. Lett.* **53** 2339

[93] Freitag *et al* 1993 *Chem. Phys. Lett.* **210** 10

[94] Gorschlüter A and Merz H 1994 *Phys. Rev.* B **49** 17293–302

[95] Castell M R, Wincott P L, Condon N G, Muggelberg C, Thornton G, Dudarev S L, Sutton A P and Briggs G A D 1997 Atomic-resolution STM of a system with strongly correlated electrons: NiO(001) surface structure and defect sites *Phys. Rev.* B **55** 7859–63

[96] Hagendorf Ch, Shantyr R, Meinel K, Schindler K-M and Neddermeyer H 2003 Scanning tunneling microscopy and spectroscopy investigation of the atomic and electronic structure of CoO islands on Ag(001) *Surf. Sci.* **532–535** 346–50

[97] Sebastian I 2000 Rastertunnelmikroskopie zur keimbildung und zum wachstum dünner CoO-Schichten auf Ag(100) und Au(111) *PhD Thesis* Martin-Luther-Universität, Halle-Wittenberg

[98] van Elp J, Wieland J L, Eskes H, Kuiper P, Sawatzky G A, de Groot F M F and Turner T S 1991 Electronic structure of CoO, Li-doped CoO and $LiCoO_2$ *Phys. Rev.* B **44** 6090–103

[99] Glöckler K, Sokolowski M, Soukopp A and Umbach E 1996 Initial growth of insulating overlayers of NaCl on Ge(100) observed by scanning tunneling microscopy with atomic resolution *Phys. Rev.* B **54** 7705–8

[100] Hebenstreit W, Redinger J, Horozova Z, Schmid M, Podloucky R and Varga P 1999 Atomic resolution by STM on ultra-thin films of alkali halides: experiment and local density calculations *Surf. Sci.* **424** L321–8

[101] Mauch I, Kaindl G and Bauer A 2003 *Surf. Sci.* **522** 27

[102] Repp J 2002 Rastertunnelmikroskopie und -spektroskopie an adsorbaten auf metall- und isolatoroberflächen *PhD Thesis* Freie Universität, Berlin

[103] Fölsch S, Helms A, Zölphel S, Repp J, Meyer G and Rieder K-H 2000 Self-organized patterning of an insulator-on-metal system by surface faceting and selective growth: NaCl/Cu(211) *Phys. Rev. Lett.* **84** 123–6

[104] Repp J, Fölsch S, Meyer G and Rieder K-H 2001 Ionic films on vicinal metal surfaces: enhanced binding due to charge modulation *Phys. Rev. Lett.* **86** 252

[105] Fölsch S, Riemann A, Repp J, Meyer G and Rieder K H 2002 From atomic kink to mesoscopic surface patterns: ionic layers on vicinal metal surfaces *Phys. Rev.* B **66** 161409

[106] Ramoino L, Schintke S, Jung T A and Güntherodt H-J 2003 at press

[107] Barjenbruch U, Fölsch S and Henzler M 1989 *Surf. Sci.* **211** 749

[108] Hebenstreit W, Schmid M, Redinger J, Podloucky R and Varga P 2000 Bulk terminated NaCl(111) on aluminium: a polar surface of an ionic crystal? *Phys. Rev. Lett.* **85** 5376–7

[109] Olsson F E and Persson M 2003 A density functional study of adsorption of sodium-chloride overlayers on a stepped and a flat copper surface *Surf. Sci.* **540** 172–84

[110] Pan F M, Verheij L K, David R and Franchy R 2001 Temperature dependence of the growth of gallium oxide on CoGA(100) *Thin Solid Films* **400** 22–5

[111] Berner U and Schierbaum K 2001 Cerium oxide layers on Pt(111): a scanning tunneling microscopy study *Thin Solid Films* **400** 46–9

[112] Nörenberg H and Briggs G A D 1998 *Surf. Sci.* **402–404** 734

[113] Wuilloud E, Delley B, Schneider W-D and Baer Y 1984 Spectroscopic evidence for localized and extended f-symmetry states in CeO_2 *Phys. Rev. Lett.* **53** 202

[114] Roessler D M and Walker W C 1967 Electronic spectrum and ultraviolet optical properties of crystalline MgO *Phys. Rev.* **159** 733–8

[115] Henrich V E, Dresselhaus G and Zeiger H J 1980 Energy-dependent electron-energy-loss spectroscopy: application to the surface and bulk electronic structure of MgO *Phys. Rev.* B **22** 4764–75

[116] Cox P A and Williams A A 1986 Surface excitons on ionic crystals *Surf. Sci.* **175** L782–6

[117] LaFemina J P and Duke C B 1991 Dependence of oxide surface structure on surface topology and local chemical bonding *J. Vac. Sci. Technol.* A **9** 1847–55

[118] Didier F and Jupille J 1994 Layer-by-layer growth mode of silver on magnesium oxide (100) *Surf. Sci.* **307–309** 587–90

[119] Schönberger U and Aryasetiawan F 1995 Bulk and surface electronic structures of MgO *Phys. Rev.* B **52** 8788–93

[120] Klaua M, Ullmann D, Barthel J, Wulfhekel W, Kirschner J, Urban R, Monchesky T L, Enders A, Cochran J F and Heinrich B 2001 Growth, structure, electronic, and magnetic properties of MgO/Fe(001) bilayers and Fe/MgO/Fe(001) trilayers *Phys. Rev.* B **64** 134411

[121] Oh H, Lee S B, Seo J, Min H G and Kim J-S 2003 Chemical structure of the interface between MgO films and Fe(001) *Appl. Phys. Lett.* **82** 361–3

[122] Martínez Boubeta C, Costa-Krämer J L and Cebollada A 2003 Epitaxy, magnetic and tunneling properties of transition metal/MgO(001) heterostructures *J. Phys.: Condens. Matter* **15** R1123–67

[123] Wu M-C, Corneille J S, Estrada C A, He J-W and Goodman D W 1991 Synthesis and characterization of ultra-thin MgO films on Mo(100) *Chem. Phys. Lett.* **182** 472–8

[124] Wu M-C, Corneille J S, He J-W, Estrada C A and Goodman D W 1992 Preparation, characterization, and chemical properties of ultrathin MgO films on Mo(100) *J. Vac. Sci. Technol.* A **10** 1467–71

[125] Xu C, Oh W S, Liu G, Kim D Y and Goodman D W 1997 Characterization of metal clusters (Pd and Au) supported on various metal oxide surfaces (MgO and TiO_2) *J. Vac. Sci. Technol.* A **15** 1261–8

[126] Rainer D R and Goodman D W 1998 Metal clusters on ultrathin oxide films: model catalysts for surface science studies *J. Mol. Catal.* A **131** 259–83

[127] Altieri S 1999 Electronic structure of oxide thin films on metals *PhD Thesis* Rijksuniversiteit, Groningen

[128] Altieri S, Tjeng L H and Sawatzky G A 2000 Electronic structure and chemical reactivity of oxide-metal interfaces: MgO(100)/Ag(100) *Phys. Rev.* B **61** 16948–55

[129] Schönberger U, Andersen O K and Methfessel M 1992 Bonding at metal-ceramic interfaces; *ab initio* density-functional calculations for Ti and Ag on MgO *Acta Metall. Mater.* **40** 1–10

[130] Li C, Wu R, Freeman J A and Fu C L 1993 Energetics, bonding mechanism, and electronic structure of metal-ceramic interfaces: Ag/MgO(001) *Phys. Rev.* B **48** 8317–22

[131] Heifets E, Kotomin E A and Orlando R 1996 Hartree–Fock simulation of the Ag/MgO interface structure *J. Phys.: Condens. Matter* **8** 6577–84

[132] Gaisch R, Gimzewski J K, Reihl B, Schlittler R, Tschudy M and Schneider W-D 1992 Low-temperature ultra-high-vacuum scanning tunneling microscope *Ultramicroscopy* **42–44** 1621–6

[133] Gaisch R 1994 Scanning tunneling microscopy in ultra high vacuum at low temperatures *PhD Thesis* Université de Lausanne, IPMC-BSP, CH-1015 Lausanne

[134] Schaffner M-H, Patthey F and Schneider W-D 1998 Growth study of silver on MgO(100)/Mo(100) *Surf. Sci.* **417** 159–67

[135] Wollschläger J, Viernow J, Tegenkamp C, Erdös D, Schröder K M and Pfnür H 1999 Stoichiometry and morphology of MgO films grown reactively on Ag(100) *Appl. Surf. Sci.* **142** 129–34

[136] Wollschläger J, Erdös D and Schröder K-M 1998 The formation of mosaics during the reactive growth of MgO films on Ag(100) *Surf. Sci.* **402–404** 272–6

[137] Valeri S, Altieri S, di Bona A, Luches P, Giovanardi C and Moia T D 2002 Thickness-dependent strain in epitaxial MgO layers on Ag(001) *Surf. Sci.* **507–510** 311–7

[138] Kiguchi M, Goto T, Saiki K, Sasaki T, Iwasawa Y and Koma A 2002 Atomic and electronic structures of MgO/Ag(001) heterointerface *Surf. Sci.* **512** 97–106

[139] Li J, Berndt R and Schneider W-D 1996 Tip-assisted diffusion on Ag(110) in scanning tunneling microscopy *Phys. Rev. Lett.* **76** 1888–91

[140] Roşu M F, Laurens C R, Falepin A, James M A, Langelaar M H, Pleiter F, Rogojanu O C and Niesen L 1998 Direct observation of the self-diffusion mechanism on the Ag(100) surface *Phys. Rev. Lett.* **81** 4680–3

[141] Kramer J, Tegenkamp C, Ernst W and Pfnür H 2003 Growth and surface morphology: epitaxial MgO films and the Ag(1, 1, 19) substrate *Surf. Sci.* **537** 265–75

[142] Valeri S, Altieri S, Del Pennino U, Di Bona A, Luches P and Rota A 2002 *Phys. Rev.* B **65** 245410

[143] Kiguchi M, Entani S, Saiki K, Inoue H and Koma A 2002 Two types of epitaxial orientations for the growth of alkali halide on fcc metal substrates *Phys. Rev.* B **66** 155424

[144] Sanchez A, Abbet S, Heiz U, Schneider W-D, Häkkinen H, Barnett R N and Landman U 1999 When gold is not noble: nanoscale gold catalysts *J. Phys. Chem.* A **103** 9573–8

[145] Heiz U and Schneider W-D 2000 Nanoassembled model catalysts *J. Phys. D: Appl. Phys.* **33** R85–102

[146] Tjeng L H, Vos A R and Sawatzky G A 1990 Electronic structure of MgO studied by angle resolved ultraviolet photoelectron spectroscopy *Surf. Sci.* **235** 269–79

[147] Stengel M and Baldereschi A 2003 at press

[148] Shluger A L, Sushko P V and Kantorovich L N 1999 Spectroscopy of low-coordinated surface sites: theoretical study of MgO *Phys. Rev.* B **59** 2417–30

[149] Wu M-C, Estrada C A, Corneille J S and Goodman D W 1992 Model surface studies of metal oxides: adsorption of water and methanol on ultrathin MgO films on Mo(100) *J. Chem. Phys.* **96** 3892–900

[150] Troullier N and Martins J L 1991 Efficient pseudopotentials for plane-wave calculations *Phys. Rev.* B **43** 1993–2006

[151] Fuchs M and Scheffler M 1999 *Ab initio* pseudopotentials for electronic structure calculations of poly-atomic systems using density-functional theory *Comput. Phys. Commun.* **119** 67–98

[152] Pickett W E 1986 Density functionals in solids: II. Excited states *Comment. Solid State Phys.* **12** 57

[153] Schuppler S, Fischer N, Fauster Th and Steinmann W 1990 Bichromatic two-photon photoemission spectroscopy of image potential states on Ag(100) *Appl. Phys.* A **51** 322–6

[154] Sgroi M, Pisani C and Busso M 1999 *Thin Solid Films* **400** 64

[155] Nagl C, Schmid M and Varga P 1996 Inverse corrugation and corrugation enhancement of Pb superstructures on Cu(111) and (110) *Surf. Sci.* **369** 159–68

[156] Lüth H 1995 *Surfaces and Interfaces of Solid Materials* 3rd edn (Berlin: Springer) ISBN 3-540-58576-1

[157] Overhauser W 1989 Band-edge detection in insulators by tunneling spectroscopy *Appl. Phys. Lett.* **54** 2490–2

[158] Bobrov K, Mayne A J and Dujarin G 2001 Atomic scale imaging of insulating diamond through resonant electron injection *Nature* **431** 616

[159] Prinz G A 1999 Magnetoelectronics applications *J. Magn. Magn. Mater.* **200** 57–68